The Effect of Multipole-Enhanced Diffusion on the Joule Heating of a Cold Non-Neutral Plasma

by

Steven Francis Chapman

A dissertation submitted in partial satisfaction of the

requirements for the degree of

Doctor of Philosophy

in

Physics

in the

Graduate Division

of the

University of California, Berkeley

Committee in charge:

Professor Joel Fajans, Chair

Professor Jonathan Wurtele

Professor Eugene Chiang

Fall 2011

The Effect of Multipole-Enhanced Diffusion on the Joule Heating of a Cold Non-Neutral Plasma

Abstract

The Effect of Multipole-Enhanced Diffusion on the Joule Heating of a Cold Non-Neutral Plasma

by

Steven Francis Chapman

Doctor of Philosophy in Physics

University of California, Berkeley

Professor Joel Fajans, Chair

One proposed technique for trapping anti-atoms is to superimpose a Ioffe-Pritchard style magnetic-minimum neutral trap on a standard Penning trap used to trap the charged atomic constituents. Adding a magnetic multipole field in this way removes the azimuthal symmetry of the ideal Penning trap and introduces a new avenue for radial diffusion. Enhanced diffusion will lead to increased Joule heating of a non-neutral plasma, potentially adversely affecting the formation rate of anti-atoms and increasing the required trap depth. We present a model of this effect, along with an approach to minimizing it, with comparison to measurements from an intended anti-atom trap.

This work is dedicated, in memory of
Doctor Mark Skalsey,
I wouldn't be here without you.

Contents

List of Figures

List of Tables

Acknowledgments

I want to thank all members of the ALPHA collaboration, past and present, for working to design, construct, maintain, and operate the experimental apparatus on which these experiments were performed.

I want to thank my committee for their patience and support.

I would like to specifically thank my adviser, Joel Fajans, for his help getting this thesis into a comprehensible and presentable state and my colleague, Alex Povilus, for his patience in listening to me ramble incoherently about concepts to be found within.

Finally, I would like to thank everyone else I've ever met, on the off chance that they've somehow contributed to the work presented herein.

Chapter 1

Introduction

1.1 Motivation

One of the fundamental tenants of much of modern theoretical physics is the CPT theorem. It states that any quantum field theory including locality, Lorentz-invariance, and a Hermitian Hamiltonian must preserve CPT symmetry [1].

The term CPT stands for the simultaneous combination of three simpler symmetries that are not necessarily preserved by such theories. However, all three were originally theorized to be preserved, until experimental evidence to the contrary was discovered.

Charge conjugation symmetry implies no change in physical law with the inversion of all electric charges. Among the four fundamental forces, only the weak interactions are known to break this symmetry.

Parity symmetry implies no change in physical law under a full reflection of the system, equivalent to reversing left and right-handedness. This symmetry is also only known to be violated by weak interactions, generally the same interactions that violate charge conjugation symmetry. In fact, it was once theorized that these were always violated at the same time, if at all.

Time reversal symmetry implies no change in physical law under a reversal of the direction of time. In contrast to the previous two symmetries, this one is, apparently, violated by a significant majority of macroscopic phenomena, thanks to the second law of thermodynamics. However, observations of microscopic violations are, so far, constrained to those few phenomena that violate one and only one of the previous two symmetries.

While it may seem that we have a relatively poor track record regarding the preservation of these symmetries, the full combination of CPT is on a notably firmer theoretical foundation. It cannot be violated without also violating Lorentz invariance. Nonetheless, it clearly behooves us to place experimental constraints on any possible violations of this symmetry.

Assuming we don't anticipate any gross violations of CPT symmetry, the best way to constrain minor violations is to find a well-understood and thoroughly-measured system that has an accessible CPT mirror, and inspect the mirrored system as well. Atomic hydrogen is such a system with atomic antihydrogen as its CPT mirror. Comparison of the $1s \rightarrow 2s$ transition in atomic hydrogen and antihydrogen would constrain CPT violation,

provided it was not actually observed, to, theoretically, one part in 10^{18} [2].

To perform such a measurement is the primary goal of the antihydrogen Laser Physics Apparatus (ALPHA) collaboration.

To date, we have successfully trapped antihydrogen [3], but have not yet attempted to perform laser spectroscopy. Even so, this preliminary achievement is notable in its own right as a technical benchmark and will also serve as a starting point for any future experiments with or practical applications of neutral systems of antimatter.

1.2 Scope

The work presented in this thesis was done entirely by members of the ALPHA collaboration working towards its overarching goals.

However, we will deal exclusively with work focused on diagnosing the temperature of our plasmas and on the degree to which applying the octupole magnet we use for trapping can change the temperature of the non-neutral component plasmas.

In the next chapter we will describe the experimental methods and apparatus used by the ALPHA collaboration with the intention of motivating our interest in the temperature of our plasmas and the effect that our trapping fields might have on it.

In practice, we find that, when we expose our non-neutral component plasmas (antiprotons and positrons) to the azimuthally asymmetric magnetic fields needed to trap electrically neutral antihydrogen atoms they often begin to expand radially at an accelerated pace. This is often accompanied with a rise in the temperature of the plasmas. For reasons that will be explained in chapter 2, we wish to avoid this effect as much as possible.

In chapter 3 we will describe, in detail, our technique for determining the temperature of our plasmas along with its limitations.

In chapter 4 we will develop a model for the expansion and heating of our plasmas in our trapping fields, with slightly greater generality than required by our specific experiment.

Finally, we will compare this model to observations.

Additionally, note that, unless otherwise stated, all quantities are in SI units.

Chapter 2

Experimental Methods

2.1 Trapping charged particles

2.1.1 General Principles

As antihydrogen is not found in nature and cannot be directly produced by any simple process, we must first procure and trap its charged constituents: antiprotons and positrons.

Charged particles are held and manipulated in a modified Malmberg-Penning trap [4]. This trap consists of a number (at least three, in concept) of coaxial, hollow, cylindrical electrodes placed end to end in a stack and immersed in a strong, ($\geq$ 1T) uniform magnetic field, provided by a superconducting solenoid, and oriented with the field parallel to the electrode axes.

Confinement along the axis of the electrodes is provided by applying potentials to the electrodes. If, in the case of the simplified 3-electrode trap, we apply a negative voltage to the two outer electrodes and a positive (in either absolute or relative terms) voltage to the central electrode we will create a potential well along the axis of the electrodes that will trap negatively charged particles up to some energy determined by the specific voltages

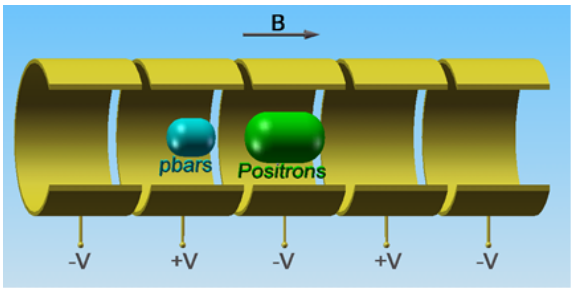

Figure 2.1: simplified depiction of a penning trap: charged particles are confined radially by the magnetic field and longitudinally by the electric fields produced by the relative biases of the electrodes. This trap is biased to confine oppositely charged particles in adjacent, single-electrode long wells.

applied and the geometry of the electrodes; provided that the electrodes are sufficiently long, compared to their radius.

Charged particles inside the cylinders are prevented from moving outward radially by the magnetic field. Kinetic energy perpendicular to the magnetic field will, instead, be directed into cyclotron motion: circular orbits perpendicular to the field with radius

$$r_c = \frac{mv}{qB} \cong (30nm)\frac{\sqrt{T}}{B} \tag{2.1}$$

for an electron with a thermal velocity.

Unfortunately, the magnetic field does not prevent all large-scale motion of the particles perpendicular to the magnetic field. Any force driving particles across the magnetic field will result in a drift velocity perpendicular to both the magnetic field and the perturbing force.

$$\vec{v_d} = \frac{\vec{F} \times \vec{B}}{qB^2} \tag{2.2}$$

By far, the most important source of additional forces is the electric field. Both the potentials applied to the electrodes and the space charge of any plasma in the trap will produce electric fields.

Fortunately, the cylindrical symmetry of our trap and, presumably, plasma ensure that all electric fields will be almost entirely radial. Thus, the drifts will be azimuthal, hopefully resulting in no significant changes in plasma distribution over time. This helps to ensure long lifetimes for the charged particles in the trap.

2.1.2 Specifics of the Trap

The actual trap used in the experiment [3] consists of roughly 35 electrodes split up into three sections used for different applications. All three sections lie inside a 1T solenoidal field. See Fig 2.2.

The first section, called the catching trap, is located on the end of the full assembly henceforth known as the "upstream" end. This section is used to "catch" high energy particles entering this region of the trap. This is done with two special electrodes located at both ends of the catching trap, which are designed with increased spacing to the electrodes on either side, so that high voltage ($\leq$ 5kV) can be applied to them safely.

The 11 electrodes in the catching trap have an inner diameter of 33.6mm and have lengths slightly less than either this diameter, or half its value. The high-voltage electrodes are, roughly, 50% longer again than the larger normal electrodes.

This region also contains one electrode that has been separated into six angular sectors that can be biased to different voltages. This allows us to apply azimuthally dependent potentials to the plasma. This is primarily used to compress or expand plasmas radially, as will be explained in section 2.3.5.

Surrounding the catching trap is a smaller, superconducting solenoid that, when energized, increases the solenoidal field in the region by up to 2T.

The central section of the trap is where antiprotons and positrons are mixed to produce antihydrogen. Thus, it is called the mixing trap. The 13 electrodes in this section

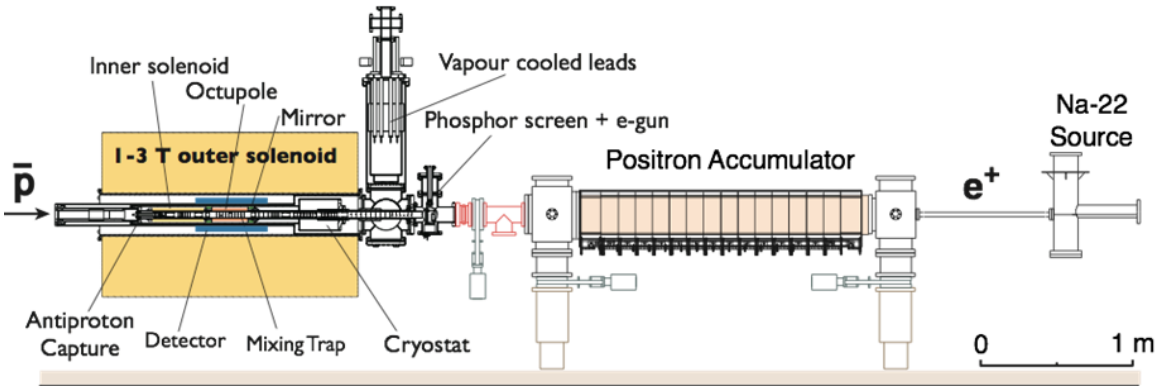

Figure 2.2: Cross-section of the ALPHA experimental apparatus: on the left (upstream) end, one sees our superconducting solenoid. The sections of Penning trap inside this solenoid are those cooled by liquid helium and are the primary site for the measurements described. All other parts of the trap, except for the moderator of the positron source, are at room temperature.

have an inner diameter of 44.55mm, but maintain the same aspect ratios as in the catching trap.

This section contains another azimuthally-sectored electrode. This electrode is cut into four sectors, instead of the six sectors in the catching trap, but the uses of the electrode are generally the same.

This section of the trap is used for mixing because it is surrounded by a configuration of additional superconducting magnets that can be used to create a local minimum of the magnetic field inside the trap. Such a field configuration is required for our approach to trapping antihydrogen. These magnetic fields are discussed in greater detail in section 2.5.

The final region of the trap, called the positron trap, is located at the "downstream" end of the electrode stack. It does not have any additional magnets associated with it and extends outside of the uniform field of the solenoid. It also contain another high-voltage electrode used to facilitate the transfer of positrons into the trap. This is discussed in greater detail in sections 2.2.2 and 2.3.3.

The electrodes in this region are generally of the same sizes as those in the catching trap. However, there are two much longer electrodes at the extremity of this trap. These "transfer" electrodes are always kept grounded, and serve the single purpose of shielding particles entering or leaving the trap on this end.

At the downstream end of the trap is an aperture with a hinged flap that we can open and close remotely. The primary purpose of this flap is to block thermal radiation. The trap itself is cryogenically cooled along with the superconducting magnets. The vacuum system beyond the aperture is, generally, not. Unobstructed line of sight between these two regions could result in an additional heat load on the order of Watts. However, while we can observe the effect of this radiation load when the flap is open, experiments indicate that it does not dominate the temperature of the traps.

The trap is cooled sufficiently that any residual gasses in the vacuum system should condense onto any free surface. Thus, the pressure in the cryogenically cooled region should be lower than in other regions. Keeping the flap closed, while it is certainly not a vacuum seal, reduces the flow of gasses into the cryogenic region, keeping the pressure lower and improving the lifetime of particles in the trap.

Beyond the aperture, there are additional transfer electrodes leading to the room-temperature region of the trap. Crossing the axis of the trap, in this region, is a linear motion feed-through that can bring various room-temperature devices into alignment with the trap. This region is also where all of our vacuum pumps connect to the system.

The positron accumulator is at the extreme downstream end of the apparatus.

2.2 Charged particle sources

2.2.1 Electrons

The electrons used in our experiment are produced by a Barium Oxide thermionic cathode. A current is passed through a tungsten wire pressed against a Barium Oxide disc, heating the disc to white-hot temperatures when in operation. The entire disc is electrically biased to a negative potential (on the order of -10V), causing emission of electrons at rates up to 1 mA.

There are also plates (with apertures, where relevant) on both sides of the cathode, along the trap axis, that can be biased to direct the electrons into the trap, preferentially, and alter the spatial spread and energy of the electron beam.

The cathode is located on the linear motion feed-through in the room-temperature region of the vacuum system. When in use, the cathode can be aligned with the axis of the trap, or intentionally misaligned. This is outside the physical interior of the main solenoid, but still inside the fringe field, at a magnitude of around 100 G.

2.2.2 Positrons

Our positrons are produced by the radioactive decay of Sodium-22. They are then reduced to controllable energies with a solid Neon moderator. Afterward, they are collected in a Surko-style differential-pumping accumulator [5].

This accumulator is located at the extreme downstream end of the experiment, on the opposite side of the linear motion feed-through and vacuum pumps from the cryogenic trap. When we want to transfer the positrons from the accumulator to the trap, we move the linear motion feed-through until a grounded cylinder is aligned with the axes of the trap and accumulator, allowing the positrons to pass through unhindered. Due to the gasses used in the positron accumulator, it is generally valved off from the rest of the experiment.

2.2.3 antiprotons

antiprotons are produced in high-energy (>1GeV) collisions in the Proton Synchrotron at CERN. During operation, regular bunches of the antiprotons are sent to the antiproton Decelerator facility, where they are reduced in energy via the same techniques

generally used to increase energy in accelerators. They are finally delivered to the experiments in the antiproton Decelerator hall at roughly 5 MeV.

As we lack the means to capture particles at energies in excess of 5 keV, we pass the bunch of antiprotons through a metal foil degrader. This has the effect of reducing the number of antiprotons in the bunch and the energy of those that remain [6]. There is an optimum, both experimentally and theoretically determined, value for the thickness of the foil that maximizes that number of antiprotons in a bunch that we can catch. This is approximately 10,000 antiprotons on a repetition time of roughly 100s.

The antiprotons enter the trap on the upstream end (which is the source of the term) and are caught in the aptly named catching trap.

2.3 Manipulating Charged Particles

2.3.1 Catching Particles

All particles enter the trap as either a beam or a free-streaming bunch. We need to find a way to contain these particles and remove their bulk kinetic energy.

To first contain the particles, we select two electrodes in the trap to bound the region in which we intend to capture the particles. For antiprotons, these are necessarily the high-voltage electrodes in the catching trap, but we have much more leeway with electrons and positrons. We then bias the bounding electrode farthest from the source of the particles in question to a voltage sufficient to stop at least some of the particles.

All remaining electrodes in the bounded region can be grounded. However, they are usually biased to some configuration that will not stop the particles, but will ease subsequent manipulations of the particles. For example, when preparing to trap electrons, which enter the trap as a largely mono-energetic beam, the region is usually biased to a voltage just below (in magnitude) that required to stop the beam. This helps to reduce the energy of the particles in the trapping region, and improves our trapping rate.

Then, once the particles are in the intended trap, the other bounding electrode is also biased, trapping the particles in between. For the antiprotons and positrons, the timing of this process is, necessarily, finely tuned experimentally. For the electrons, we merely need to wait for the continuous electron beam to fill the trapping region as well as it can.

2.3.2 Cyclotron Cooling of Particles

Having contained the particles in the trap is not terribly helpful if they still have tens or thousands of electron volts in energy. Luckily, the particles are in an, at least, 1T magnetic field and will begin to cyclotron cool, according to

$$\frac{\partial T}{\partial t} = -\frac{2q^4}{9\pi m^3 \epsilon_0 c^3} B^2 T \tag{2.3}$$

It is important to remember that cyclotron cooling only works to reduce the energy of particles in motion perpendicular to the magnetic field, while we are concerned here with reducing energy parallel to the magnetic field. Thus, this will only work if the particles are

sufficiently collisional that the temperatures of the particle ensemble both perpendicular and parallel to the magnetic field are equal.

For electrons and positrons in a 1T field, this process results in an exponential decay of the temperature to some equilibrium with a time constant of roughly 4s. This equilibrium is set by all sources of heating to the plasma. Common sources are thermal radiation from the electrodes and electronic noise on the same. Lepton plasmas in our trap generally cooled to somewhere between 100K and 10K (1meV), by this process, with a theoretical limit of 4K- set by the temperature of the cryogens used to cool the trap.

However, if one notes the dependence of the cyclotron cooling rate on the particle mass, it is clear that the process will not cool antiprotons on a reasonable timescale.

To cool antiprotons, we first prepare an electron plasma in a smaller well inside the larger well in which we first catch the antiprotons The antiprotons undergo a process called sympathetic cooling [7]. The relatively hot antiprotons collide with the electrons and transfer some of their kinetic energy. The electrons then cyclotron radiate the energy away. This allows the antiprotons to cool to the same equilibrium temperature as the electrons at a rate comparable to the slower of the electron cyclotron cooling rate and the electron-antiproton collision rate.

2.3.3 Moving Particles

If we would prefer trapped particles to be somewhere other than where they happen to be trapped, we have two main techniques for getting them there.

We can attempt a controlled movement of the plasma. This is accomplished by gradually altering the potentials biasing the electrodes, until the final configuration produces a trap for the plasma in the desired location, or of the desired shape. Of course, care must be taken to ensure that particles are not lost during the process.

Operations of this sort almost universally result in some heating of the trapped plasma, due to energy added by the electric fields produced during the potential changes. As a result, we usually follow all full movements with a wait for cyclotron cooling to take effect. As this will not work if we're moving antiprotons, we usually only move those particles in this manner while they are still trapped in the same well as an electron plasma, allowing for sympathetic re-cooling.

We can also enact a slightly more dramatic movement, called a dump. The end result of the potential manipulations of a dump are that the plasma leaves containment with all electrodes in one direction at a relative negative bias to the energy of the particles and at least the one adjacent electrode in the other direction at a strong relative positive bias. This results in the plasma free-streaming at some controlled energy in a particular direction.

A dump is generally used to remove particles from the trap entirely, though an analogous process is used to transfer the positrons from their accumulator into the trap.

There are two classes of techniques for enacting a dump, which are chosen between based on the needs of the particular case. The first is to raise all of the electrodes involved in trapping a plasma to a positive energy relative to ground, then simply lower the potential on the bounding electrode(s) in one direction. The second is to arrange the potentials of

the trap so that the potential barrier is larger in one direction than the other, then increase the potential of the interior, non-bounding electrodes.

While attempting to dump particles, it is important to remember that electrons and positrons travel roughly forty times faster than antiprotons at the same temperature. We take advantage of this fact when we need to remove the electrons used to sympathetically cool the antiprotons before the latter are mixed with positrons (lest all our positrons be annihilated). A sufficiently swift dump and return to the original well will allow the electrons to escape while the majority of the antiprotons will remain trapped, though they will almost certainly be slightly heated.

2.3.4 Evaporative Cooling

It is often the case that we would like to reduce the temperature of the cloud of antiprotons without adding electrons, or reduce the temperature of our lepton plasmas below the normal equilibrium. To accomplish this, we can, at least attempt to, use evaporative cooling [8].

To evaporatively cool a plasma, we enact a slow, partial dump. That is, we manipulate the potentials as if performing a dump, but don't follow through until the plasma is completely free of the trap. If the depth of the trap is correctly tuned to the space charge of the plasma, only particles with a higher-than-average kinetic energy can escape the trap. This results in the average energy of the plasma, and therefore the temperature, decreasing; at the cost of fewer remaining particles. However, we can experimentally confirm that the number of particles with kinetic energy corresponding to a temperature below a given value (say 1K), is increased by this process.

2.3.5 Rotating Wall Manipulation

As previously mentioned, a major strength of a Penning-style trap is that the cylindrical symmetry of the trap prevents torques on the plasma, which would likely result in radial expansion and eventual losses. However, by applying controlled torques, we can alter the radial profile of the plasma to our benefit.

Both the catching and mixing traps contain electrodes cut into angular sectors. If we apply oscillating potentials to each sector, with phase offsets between sectors corresponding to the angular size of the sectors, we can effectively create an electric field in the trap that rotates azimuthally. We call this setup a rotating wall. Generally, if the rotation of the electric field is in the same direction as and at roughly the same rate as the ordinary $E \times B$ rotation of the plasma, we can smoothly either increase or decrease the size of a plasma in the trap [9].

As an example of when this would be useful, consider the trapping of antiprotons The size of the antiproton cloud entering the trap is much larger radially than both the eventual size that we want for the antiproton cloud and the electron plasmas we typically prepare. antiprotons that do not spatially overlap the electron plasma do not cool and cannot be trapped. But we can use the rotating wall to increase the size of the electron plasma, increasing the number of antiprotons we cool. Then, we can compress the electron plasma back down to the desired size.

Note that this technique generally does not work on our antiproton clouds on their own, as they generally lack enough charge to produce a significant electric field. However, when immersed in an electron plasma, the antiprotons distribution follows the electron distribution, by and large, during compression or expansion.

2.4 Diagnosing Charged Particles

2.4.1 Faraday Cup

The most basic possible diagnostic of the particles is a check of whether or not we've managed to trap any. We can check the number of charged particles in the trap with a diagnostic device we call the Faraday cup.

To use the diagnostic, we simply dump particles towards the upstream end of the trap. They will impact the final antiproton degrader, an electrically isolated foil connected to an amplifier. This foil can be electrically biased to potentially improve extraction of a particular particle species. Thus, provided we can determine the capacitance of the entire assembly, we can directly relate the signal to charge impacting the foil.

Unfortunately, the behavior of this diagnostic is not necessarily consistent for various particle species. When the antimatter particles impact on the foil, their annihilation may release sufficient energy to eject charged particles from the foil. As the resolution of our implementation of this diagnostic was only on the order of a million particles, however, we never observed this variation across particle species via this diagnostic.

2.4.2 Microchannel Plate

The Faraday cup diagnostic has two major downsides. First, it is not terribly precise. A resolution of only a million particles leaves it unable to even detect most of our antiproton clouds. Second, it tells us little or nothing about the distribution of the plasmas. For tasks where the Faraday cup is insufficient, we also have a Microchannel plate (MCP) assembly.

The assembly consists of the MCP itself and a phosphor screen. The MCP amplifies charge that impacts its front surface, while maintaining its two-dimensional spatial distribution. The phosphor screen then converts the amplified charge into light. This, combined with a mirror and a CCD camera, allows us to visually determine the spatial distribution of a particle cloud in the trap, integrated along the trap axis.

This information, if combined with a detailed knowledge of the potentials produced by the electrodes, allows one to numerically compute the full spatial distribution of the cloud, if desired.

The MCP itself is a plate filled with small (15 μm) channels through it. When in use, the front of the plate is electrically biased to draw in the particles being diagnosed, usually to $\pm$ 100V.

The back of the plate is biased to a positive voltage, relative to the front plate. When a particle impacts the wall of a channel with sufficient energy, it may kick out electrons into the channel. These electrons are accelerated down the channel by the electric field between the front and back plates of the MCP. However, these channels are at an angle

relative to this field, so the electrons typically impact the channel wall again, potentially kicking out even more electrons. Thus, by tuning the voltage difference across the MCP, we can scale the number of electrons leaving the back of the plate for every charge hitting the front of the plate: the charge gain of the MCP.

Of course, there is a limit on the number of electrons that can be provided by a given channel over the time scale of a single measurement. If this limit is exceeded, either due to too high a gain or too many particles hitting the front of the plate, the MCP saturates and most information is lost.

The phosphor screen is, itself, biased to a positive voltage relative to the back of the MCP to accelerate the electrons leaving the MCP onto its surface. The harder the particles hit the phosphor screen, the more light released by the impact. Thus, the relative voltage between the MCP and the phosphor screen can be tuned to adjust the light gain, with the goal of making the image bright enough to be easily seen without saturating the CCD camera.

Of course, the behavior of the various species of particles differ when impacting the front of the MCP. For example, antiprotons typically annihilate, spraying decay products in all directions, including across nearby channels or out of the MCP entirely. However, unlike with the Faraday cup diagnostic, we have sufficient resolution to observe and characterize these effects, allowing us to correct for them [10].

In addition to determining the spatial distribution of a particle cloud, the MCP can also be used as a sensitive charge counting device by measuring the change in the voltage of the back of the MCP as the electrons escape to the phosphor screen. At maximum charge gain, we can very nearly detect a single electron. Unfortunately, as the two possible uses for the MCP assembly generally require very different biasing voltages, we cannot generally perform both measurements at the same time.

The MCP is located on the linear motion feed-through with the electron source. Thus, when we want to use the device, we align the MCP with the trap axis and bias the assembly, depending on the specific use intended.

2.4.3 Modes

In addition to applying voltages to the electrodes, we can also monitor the voltage on them. There are two main sources of induced voltages of the electrodes: capacitive coupling from other electrodes and coupling to the electric field of a plasma in the trap.

If we perturb a trapped plasma by adding a small, varying potential to one of the confining potentials, the plasma will presumably respond by changing shape or position over time. The plasma should preferentially respond at frequencies corresponding to its various modes of oscillation around whatever equilibrium it happens to be in [11]. By carefully monitoring the coupling of the plasma to an electrode other than the one being used to perturb it, we can determine the frequencies of these modes and, thereby, determine a wide variety of information about the plasma, such as its shape or temperature.

The major advantage of this diagnostic is that it does not destroy the plasma, which can then be used for other measurements afterward. Therefore, it can be a useful check of the trial to trial consistency of experiments.

Unfortunately, this diagnostic also requires a detailed theoretical model of the plasma, if you want any information more detailed than whether or not there *is* a plasma in the trap. As we were not convinced that we had such a model in a sufficiently robust state, we generally did not use this diagnostic.

2.4.4 Annihilation Detection

One limitation of the afore-mentioned diagnostics is that they largely rely on the electric charge of the particles being diagnosed. That is, they are generally less able to diagnose antiprotons, due to our usually not having as many of them. However, it is far easier to detect the absorption of an antiproton if, instead of measuring its direct charge, we look for its decay products.

Annihilations of an antiproton with a proton at low energies typically result charged pions [12], with sufficient kinetic energy to easily leave the entire trap and pass outward through the vacuum system and magnets.

Surrounding the innermost magnets, we have a silicon vertex detector [13]. It consists primarily of a multilayer array of short strips of doped silicon, biased so that any charged particle passing through a strip produces, with some efficiency, a detectable ionization current. As a charged pion passes through this detector, it must pass through several strips, allowing us to determine the path of the particle through the detector and extrapolate its path back into the trap. If an annihilation produces multiple charged pions, we can follow the multiple paths back to their intersection point, where the antiproton originally annihilated.

Thus, we can reconstruct the spatial distribution of antiprotons, when they annihilated, as well as an estimate of the total number. Also, due to the somewhat involved vertex reconstruction procedure, the measurement has a very low background. Cosmic rays pass through and trigger the detector, but their paths, when reconstructed, are almost always inconsistent with an antiproton annihilation.

Outside of the main solenoid, we also have several scintillator detectors surrounding the experiment. These consist of a large slab of scintillator attached to a photo-multiplier tube (PMT). Light is produced when a charged particle passes through the scintillator, which is picked up and amplified by the PMT and then converted to an electrical signal. Unfortunately, these detectors have no spatial resolution outside of having finite size and are generally only used for counting the number of antiproton annihilations.

With all of these diagnostics, we can detect the annihilation of a single antiproton with an efficiency of roughly 50%.

2.5 Trapping Neutral Systems

Unfortunately, our Penning-style trap is completely unable to also trap the neutral anti-atoms we produce. A neutral atom is unaffected by the electric field produced by the electrodes, provided that the field is not strong enough to ionize the atom, and is unaffected by a constant magnetic field. Thus, without modifications to the trap, any antihydrogen produced will immediately begin drifting towards the electrode wall, where it will annihilate.

However, an antihydrogen atom will have a magnetic moment, depending on which atomic state it happens to be in [14]. Thus, it will feel a force from any gradient in the magnetic field and can potentially be trapped in a local minimum of the magnetic field.

Producing a magnetic gradient along the axis of the trap is relatively simple. A short magnetic coil, called a mirror coil, placed around the trap will produce a magnetic field that is a maximum, along the axis of the trap, in the center of the coil. Two such coils, placed sufficiently far apart along the axis of the trap, will create a local minimum of the magnetic field between them.

We produce a radial magnetic gradient with a multipole magnet. An ideal n-pole magnet consists of n infinite, parallel wires arranged, evenly-spaced around a cylinder. Each wire carries the same current, but the direction of the current reverses between adjacent wires. Of course, such an arrangement is only possible for even n, and multipoles will henceforth be characterized by their order $\alpha \equiv n/2$, radius R, and field strength β. For an ideal multipole, $\beta = \frac{\alpha\mu_0 I}{2\pi R}$. Such an arrangement produces a magnetic field inside the cylinder,

$$\vec{B} = \beta \left(\frac{r}{R}\right)^{\alpha-1} \left(\cos(\alpha\theta)\hat{\theta} + \sin(\alpha\theta)\hat{r}\right) \tag{2.4}$$

Note that the magnitude of this field

$$\left|\vec{B}\right| = \beta \left(\frac{r}{R}\right)^{\alpha-1} \tag{2.5}$$

is a minimum in the center of the trap.

Of course, our physical multipole is not infinite in length and consists of wires with finite thickness. Thus, this is only approximately the field produced. However, so long as the particles are near both the radial and longitudinal center of the magnet, the approximation is good to within a few percent.

It is also important to make sure the addition of the mirror coil and multipole fields, particularly the end-effects caused by our physical multipole, does not result in local minima of the magnetic field off axis, where otherwise trapped atoms would be able to escape the trap. However, this is merely a matter of careful magnet design followed by thorough field-mapping [15].

Thus, by energizing both the mirror coils and the multipole, we can produce a local minimum of the magnetic field that will trap any sufficiently cold anti-atoms in an appropriate atomic state that happen to be inside it.

2.6 Superposition

As we can produce both a trap for charged particles and a trap for neutral atoms, the simple solution is simply to put them together. Unfortunately, the addition of one affects the other.

The depth of the neutral trap is set by the integral of the gradient of the magnetic field from the center of the trap to the point of easiest escape. That will be equal to the difference between the magnetic field magnitude in the center of the trap and the least of the field in the center of the mirror coils or the field at the electrode wall from the multipole.

Due to a combination of geometric and technological constraints our multipole, an octupole, is the weaker point in our magnetic-minimum trap. If we assume that the radius of the electrodes is very near the radius of the multipole magnet, the depth of the trap will be

$$\Delta |B| = \sqrt{B_0^2 + \beta^2} - B_0 \tag{2.6}$$

where B_0 is the magnetic field produced by the background solenoid of the Penning trap.

Thus, when designing such a superposition of traps, one has to decide both how weak the Penning trap's solenoid needs to be relative to the multipole (as the former will almost certainly not be as constrained by technology as the latter) to maintain a reasonable neutral trap depth and how weak it can be while still maintaining confinement for charged particles.

In the ALPHA experiment, we decided on a minimum solenoidal field of 1T and produced an octupole magnet with a maximum tested field of nearly 2T at the wall. The energy depth of the well is simply the product of the field depth and the magnetic moment of ground state antihydrogen, giving an energy depth on the order of 0.7K. Of course, atoms in excited states are likely to have much larger magnetic moments and can be trapped at higher energies, but will be lost eventually if they do not cool before reaching the ground state.

Regardless, as the walls of our trap are only cooled by standard liquid helium, 4K is the minimum temperature we would ever expect to see for any atoms we produced. Thus, at the very best, we would still only expect to be able to trap a small fraction of any total sample we produced.

Additionally, the gradient added to the magnetic field for trapping atoms will also affect charged particles. When energized, the mirror coils will have a tendency to reflect insufficiently energetic charged particles that we attempt to pass through them, limiting our ability to transport particles in the trap. The multipole will also produce magnetic field lines that diverge into the electrode walls. Thus, if we have a plasma with a sufficiently large radius or in a sufficiently long well, particles will be lost almost immediately by annihilation on the walls [16].

Thankfully, these effects can be minimized by keeping our plasmas small and limiting their movement through the neutral trap when it is energized. Though, this does greatly limit our ability to diagnose charged particles when they are inside the neutral trap.

A slightly more subtle complication is that a multipole field is not azimuthally symmetric. Thus, the symmetry of the Penning trap is broken and radial transport may be significantly enhanced, a topic that will be covered, in detail, in a later chapter.

Chapter 3

The Temperature Diagnostic

3.1 Principles of the Temperature Diagnostic

Note: Our temperature diagnostic was inspired, almost entirely, by the work of Dr. Brett Beck as recorded in his dissertation [17]. Sections 1-3 are a re-derivation of this work.

By definition, the temperature of a plasma is related to the distribution of kinetic energy of its constituents. As we reduce the depth of the well containing the plasma, those particles with the highest energy along the direction of the magnetic field will escape first. So, by carefully recording both the number of particles to escape and the depth of the well over time, we can, in theory, determine the temperature of a plasma.

3.1.1 Equilibrium

The most fundamental assumption required for the temperature diagnostic is that the plasma has a single temperature. That is, the plasma, or at least the portion of it that the diagnostic samples, is in global thermal equilibrium. More specifically, we assume that the distribution of kinetic energy along the direction of the solenoidal magnetic field is a Maxwell-Boltzmann distribution.

The plasma reaches and maintains equilibrium via collisions. Thus, to maintain the validity of our assumption, we must ensure either that all manipulations of the plasma prior to measurement occur on a time scale slower than the collision time or that no measurements are taken until the plasma has had many collision times over which to approach equilibrium.

An important consequence of this assumption, when combined with the intended geometry of our apparatus, is that no parameters in the plasma will vary azimuthally. Thus, we will largely ignore the angular coordinate.

3.1.2 Energy Precision

Our second fundamental assumption is a definite relation between the energy of a particle and whether or not it escapes the well. Specifically, we assume that particles escape the trap if and only if they satisfy $\frac{1}{2}mv_{||}^2 + q\Phi(r) > qV_b$, where $v_{||}$ is the particle velocity parallel to the magnetic field (in the longitudinal center of the trap) and $\Phi(r)$ is the depth

of the plasma space charge. Since the effective potential depth of the well is $V_b - \Phi$, this is essentially requiring that escaping particles have kinetic energy in the center of the trap greater than the total potential energy needed to escape it.

Since we change V_b at only one end of the trap, matching this assumption requires that we conduct the actual measurement over a time scale slow compared to the bounce time. Otherwise particles escaping the trap at a given time will actually possess a range of energies, equal to roughly $2q\tau_b\frac{\delta V_b}{\delta t}$, greater than the value corresponding to the current V_b depending on where the particles happened to be, longitudinally, in the trap when V_b passed through the value corresponding to their energy. Granted, this effect will always be present, but if $\tau_b\frac{\delta V_b}{\delta t}$ is small enough, we can safely neglect it.

This assumption also requires that the energy of an individual particle parallel to the magnetic field does not change significantly over the course of the measurement. Specifically, we require that the measurement is fast compared to a collision time.

During the course of the measurement, the plasma is necessarily not in global thermal equilibrium, as the higher energy particles are being preferentially removed. If there is time for collisions to repopulate the higher energy states, the loss of particles will be higher than expected in this model. Also, the effective temperature of the remaining plasma will be decreased by what is, essentially, evaporative cooling; adding another complication to the model. Of course, it is possible, if difficult, to correct for these effects, but it requires a knowledge of the properties of the plasma that is rather more precise than we would like to constrain ourselves with.

Combining these two caveats results in the realization that this particular model is only applicable for plasmas in which the collision rate is much slower than the bounce rate.

3.1.3 Length Effects

Another, less vital, assumption of the temperature diagnostic is that the plasma is of infinite length. This is, for any effects that are dependent on the length of the plasma, we take the limit as the length goes to infinity, in which such effects generally go to zero.

We are generally interested in the temperatures of plasmas that are well-confined. A plasma that is undergoing the diagnostic is necessarily not well-confined. Thus, the shape of the well changes both before and during the diagnostic, resulting in an increase in the length of the plasma.

As these manipulations cause a finite, absolute change in the length of plasma, there will be no effective change in a plasma of infinite length, which the model assumes. Unfortunately, many of the plasmas used in our actual experiments were short enough that numerical calculations suggest deviations from the model on the order of tens of percent. However, corrections to these effects can, luckily, be applied after the measurement, and do not alter the derivation of the model.

Another class of finite-length effects comes from our neglect of any longitudinal variation in the plasma parameters. In a long plasma, we expect the density, space charge, and the like to be constant, except at the ends of the plasma. And when the plasma is sufficiently long, the ends of the plasma, where such parameters are necessarily changing quickly to maintain continuity between parameters inside and outside of the plasma, contribute a

negligible effect. Even for a shorter plasma, our derivation will remain largely valid, assuming all plasma parameters mentioned can be considered in the longitudinal center of the plasma only.

3.1.4 Radial Variation

The model also completely neglects any radial variation in the temperature of the plasma or the blocking potential.

One would not expect any spatial variation in the temperature of the plasma, as we've already assumed that it is in global thermal equilibrium.

On the other hand, V_b certainly does vary with radius, less so if one utilizes a blocking electrode that is very long compared to its radius.

Thankfully, due to the nature of the diagnostic, we need only neglect radial variations out to a finite radius, on the order of the Debye length, for the model to retain validity. The space charge of the plasma will be highest in its radial center. For a given applied electrode excitation, V_b will be lowest in the radial center of the trap, which coincides with the center of the plasma. The diagnostic is only intended to sample the highest energy particles, and is only applied to the earliest particles to leave the trap. Thus, the diagnostic will only sample particles out to some finite radius and we only need to neglect radial variations out to this radius, which we must ensure is, in fact, small compared to the size of the actual plasma.

Similarly, any parameter that varies with radius will, by symmetry, be either a maximum or a minimum in the center of the plasma. Thus, near the center, radial variation of parameters will be reduced by virtue of having a first derivative of zero.

3.2 High-Temperature Diagnostic

3.2.1 Derivation

The space charge of the plasma is, of course, due to the electric charge of its constituent particles. Thus, as particles escape during the diagnostic, the space charge of the plasma will decrease. In order to derive a relatively simple model for the number of particles escaping from a well as a function of V_b, we will, for now, neglect this effect.

This is not terribly unreasonable, as the diagnostic is only intended to sample the first particles to escape. As these will, generally, be only a small fraction of the particles in the plasma, the change in the space charge should be negligible.

Unfortunately, this condition becomes harder and harder to preserve for colder plasmas. As the particles become more concentrated in states of lower energy, the energy resolution required to release only a small fraction of them becomes higher and higher. Eventually, one will reach the limits of their apparatus and no longer be able to extract particles without substantially changing the space charge. However, for sufficiently hot plasmas, this is not a concern.

So, we begin by assuming that the distribution of velocities parallel to the magnetic

field follow a one-dimensional, normalized Maxwell-Boltzmann distribution:

$$n(v_{||}) = n_0\sqrt{\frac{2m}{\pi k_B T}}e^{-\frac{mv_{||}^2}{2k_BT}}. \tag{3.1}$$

To determine the number of particles that have escaped, we simply integrate this distribution over all velocities greater than $\sqrt{(V_b-\Phi)\frac{2q}{m}}$. Considering only a specific radius yields

$$\begin{aligned} dN_e(r) &= 2\pi r\,dr\,l_p\,n(r)\int_{\sqrt{(V_b-\Phi)\frac{2q}{m}}}^{\infty}\sqrt{\frac{2m}{\pi k_B T}}e^{-\frac{mv_{||}^2}{2k_BT}}dv_{||} \\ &= 2\pi r\,dr\,l_p\,n(r)\,\mathrm{erfc}\left[\sqrt{(V_b-\Phi)\frac{q}{k_BT}}\right] \\ &\equiv 2\pi r\,dr\,l_p\,n(r)\,\mathrm{erfc}(\gamma), \end{aligned}$$

where we have used the complimentary error function, $\mathrm{erfc}(x) \equiv \frac{2}{\sqrt{\pi}}\int_x^\infty e^{-t^2}dt$, and defined $\gamma^2 \equiv (V_b-\Phi)\frac{q}{k_BT}$, the parallel kinetic energy (measured at the longitudinal center of the trap) required to escape the trap, normalized to the thermal energy of the plasma.

To determine the total amount of escaped charge, we simply integrate this expression over all radii. Though, due to the finite nature of our plasma, it suffices to integrate out to some arbitrarily large radius, R.

$$N_e = 2\pi l_p\int_0^R n(r)\cdot\mathrm{erfc}(\gamma)\cdot r dr. \tag{3.2}$$

We expect that N_e will depend roughly exponentially on V_b in the region of interest. In such a case, the ratio of its derivative to its value will give us the exponential dependence.

$$\frac{1}{N_e}\frac{\partial N_e}{\partial V_b} = \frac{\partial}{\partial V_b}\ln(N_e) = \frac{\int_0^R n(r)\frac{\partial}{\partial V_b}\mathrm{erfc}(\gamma)}{\int_0^R n(r)\mathrm{erfc}(\gamma)}. \tag{3.3}$$

Combining the chain rule for differentiation and the fundamental theorem of calculus with the definition of the complimentary error function and γ gives us that

$$\begin{aligned} \frac{\partial}{\partial V_b}\mathrm{erfc}(\gamma) &= \frac{\partial\gamma}{\partial V_b}\frac{\partial}{\partial\gamma}\mathrm{erfc}(\gamma) \\ &= \frac{q}{2\gamma k_BT}\frac{2}{\sqrt{\pi}}\frac{\partial}{\partial\gamma}\int_\gamma^\infty e^{-t^2}dt \\ &= \frac{-q}{\sqrt{\pi}k_BT\gamma}e^{-\gamma^2}. \end{aligned}$$

So now, if we also apply our prior assumptions about the lack of radial variation in T, we have

$$\frac{\partial}{\partial V_b}\ln(N_e) = \frac{-q}{\sqrt{\pi}k_BT}\frac{\int_0^R n(r)\frac{1}{\gamma}e^{-\gamma^2}}{\int_0^R n(r)\mathrm{erfc}(\gamma)}.$$

We further simplify by applying an asymptotic expansion of the complementary error function, valid for large arguments.

$$\mathrm{erfc}(x) = \frac{e^{-x^2}}{x\sqrt{\pi}}\left(1 - \frac{1}{2x^2} + \frac{3}{4x^4} - ...\right).$$

For values of $x \geq 2$ the terms after the first contribute less than 10%. Since we are only interested in large values of γ - or particles with energy far in excess of the thermal average - we will drop all but the first term in the expansion, yielding

$$\frac{\partial}{\partial V_b}\ln(N_e) \approx \frac{-q}{k_B T}\frac{\int_0^R n(r)\frac{1}{\gamma}e^{-\gamma^2}}{\int_0^R n(r)\frac{1}{\gamma}e^{-\gamma^2}} = \frac{-q}{k_B T}. \tag{3.4}$$

3.2.2 End of the High-Temperature Limit

It is helpful to have a more concrete understanding of the conditions where the high-temperature diagnostic is applicable than simply saying $\gamma \geq 2$. We can, instead, consider the total amount of charge we expect to escape before our condition on γ is violated.

Once again, the total number of escaped charges at a given radius is given by

$$dN_e(r) = 2\pi\, r\, dr\, l_p\, n(r)\,\mathrm{erfc}(\gamma).$$

In order to determine how γ varies with radius, we'll have to assume a density distribution for the plasma. If we assume that the plasma density is constant in the center of the plasma, at least out to a distance of several Debye lengths, we can determine the space charge of the plasma ($\Phi(r)$) and write

$$\Phi(r) = \Phi(0) - \frac{qn(0)}{4\epsilon_0}r^2.$$

We know that γ will be lowest in the radial center of the plasma. Thus, taking the condition that $\gamma \geq 2$ everywhere to its limit sets the value of $\Phi(0)$.

$$\begin{aligned}
\gamma &= \sqrt{\frac{q}{k_B T}(V_b - \Phi(r))} \\
2 &= \sqrt{\frac{q}{k_B T}(V_b - \Phi(0))} \\
\gamma^2 &= \frac{q}{k_B T}\left(4\frac{k_B T}{q} + \frac{qn(0)}{4\epsilon_0}r^2\right).
\end{aligned}$$

If we rephrase this in terms of the Debye length, we can write the total number of escaped charges at a given radius as

$$dN_e(r) = 2\pi\, r\, dr\, l_p\, n(r)\,\mathrm{erfc}\left(\sqrt{4 + \left(\frac{r}{2\lambda_D}\right)^2}\right).$$

This also helps to make clear why we only care about the density of the plasma within a few Debye lengths of the radial center. The amount of charge escaping at a given radius will be roughly exponentially damped over a scale comparable to a Debye length.

Regardless, to determine the maximum amount of charge we can expect to extract without invalidating the high-temperature diagnostic, we merely have to integrate this expression. We can, in principle, do this over all radii or out to some, sufficiently large, radius.

$$N_e = 8\pi\lambda_D^2 l_p n(0) \int \operatorname{erfc}\left(\sqrt{4+x^2}\right) x dx$$

Here we have defined a scaled coordinate ($x \equiv r/2\lambda_D$) to move all dimensional parameters outside of the integral. The value of the integral is approximately 2.15×10^{-3}.

Thus, we can interpret this result to say that we can extract only around 2% of the particles within a single Debye length of the center of the plasma without invalidating the high temperature diagnostic.

It is also useful to note that the product of the plasma density and the Debye length squared is, in fact, independent of the plasma density and is linearly proportional to the plasma temperature.

3.3 Low-Temperature Diagnostic

As we've just seen, for colder plasmas, it will become more and more technically difficult to extract sufficient charge to make a measurement while keeping $\gamma \geq 2$, and we can no longer neglect the change in space charge as particles escape. As we would still like to be able to measure the temperature of these plasmas, we require a more accurate model.

3.3.1 New Assumptions

In order to correct for the change in space charge due to escaping charge, we will need to know the radial distribution of escaping charge, in addition to the initial radial distribution of the plasma. Unfortunately, we cannot know this a priori and will need to make some additional simplifying assumptions. This assumption will be to neglect radial variation in the initial plasma density.

Initially, this may seem like an absurd assumption, as the fact that our plasma is necessarily finite in radial extent requires that its density varies with radius. However, as we demonstrated in the previous section, charge will preferentially escape from near the radial center of the plasma. Specifically, for the case of a constant density distribution, the density of the charge that escapes during the diagnostic will scale with radius as $\operatorname{erfc}\left(\sqrt{4+(r/2\lambda_D)^2}\right)$. If we integrate this out, we see that charges escaping at a radius of greater than 5 Debye lengths will be less than one part in 10^{10} of all escaping charge. Thus, so long as the plasma Debye length is much smaller than the radial extent of the plasma, we are justified in neglecting any charge escaping outside this radius. And since this means we're only concerned with the plasma very close to the radial center, where the

plasma density is constant to first order, we can safely neglect radial variation in the plasma density.

3.3.2 Derivation

Thanks to the principle of superposition, we know that the change in space charge (Φ_e) resulting from the escape of charges (n_e) is simply going to be the potential produced by said charges before they escaped, assuming that we don't release enough charge to cause large-scale reorganization of the plasma.

So,

$$\nabla^2 \Phi_e = \frac{q}{\epsilon_0} n_e(r). \tag{3.5}$$

While deriving Equation 3.2, we found that

$$\begin{aligned} n_e(r) &= n_0 \text{erfc}\left(\sqrt{\frac{q}{k_B T}(V_b - \Phi(r))}\right) \\ &= n_0 \text{erfc}\left(\sqrt{\frac{q}{k_B T}(V_b - \Phi_0(r) + \Phi_e(r))}\right), \end{aligned}$$

where the subscript 0 denotes the value of quantities before any particles escape.

Since we're only considering the plasma within a small distance of the radial center and are neglecting radial variation in the density within that range, we can write that

$$\begin{aligned} \Phi_0(r) &= \Phi_0(0) + \frac{q n_0}{4\epsilon_0} r^2 \\ &= \Phi_0(0) + \frac{k_B T}{4\pi\epsilon_0 q}\left(\frac{r}{2\lambda_D}\right)^2, \end{aligned}$$

where we've used the value of the Debye length, $\lambda_D^2 = \frac{k_B T}{4\pi q^2 n}$.

Now, our differential equation becomes

$$\nabla^2 \Phi_e = \frac{q n_0}{\epsilon_0} \text{erfc}\left(\sqrt{\frac{q}{k_B T}(V_b - \Phi_0(0) + \Phi_e(r)) + \frac{1}{4\pi\epsilon_0}\left(\frac{r}{2\lambda_D}\right)^2}\right).$$

To simplify, we make two substitutions. We define a scaled coordinate, $x \equiv \sqrt{\frac{1}{4\pi\epsilon_0}}\frac{r}{\lambda_D}$ and a scaled potential, $\Psi \equiv \frac{q}{k_B T}(V_b - \Phi_0(0) + \Phi_e)$.

This leaves us with

$$\nabla_x^2 \Psi = -\text{erfc}\left(\sqrt{\Psi + \left(\frac{x}{2}\right)^2}\right), \tag{3.6}$$

or with azimuthal symmetry and ignoring end effects,

$$\left(\frac{\partial}{\partial x} + \frac{1}{x}\right)\frac{\partial \Psi}{\partial x} = -\text{erfc}\left(\sqrt{\Psi + \left(\frac{x}{2}\right)^2}\right). \tag{3.7}$$

There is, not surprisingly, no analytic solution to this differential equation, but it can be integrated numerically, provided we have appropriate boundary conditions. That is, we now know $\Psi(x)$, provided we know $\Psi(0)$ and $\Psi'(0)$.

Determining $\Psi'(0)$ is rather trivial, as $\Psi'(0) = \frac{q}{k_B T}\Phi_e'(0)$. Due to the symmetry of the problem, the potential contribution from the escaped charge must be either a maximum or a minimum at r=0. Either way, we have that $\Psi'(0) = 0$.

To determine the boundary condition for the value of Ψ, we merely need to maintain consistency with the applied voltage on the electrode walls. As the voltage applied to the electrodes is not changed by the escape of charge from the trap, though our power supplies may be required to supply current to maintain this situation, it must be that $\Phi_e(R_w) = 0$.

We can, in principle, use this information to determine $\Phi_e(0)$ and, thereby, $\Psi(0)$. Unfortunately, we would first need to know n_e as a function of radius, which is what we're trying to determine in the first place.

We make the simplifying assumption that all escaped charge comes from within some radius, r_m and in an azimuthally symmetric distribution. From Gauss' Law, we conclude that

$$\Phi_e(r_m) = \frac{qN_e}{2\pi\epsilon_0 l_p} \ln\left(\frac{R_w}{r_m}\right).$$

So, now we can numerically determine $\Psi(x)$, provided we know the total amount of escaped charge: the quantity of actual interest.

To develop an expression for the total amount of escaped charge, we start by substituting our new variables into our expression for the escaping charge distribution:

$$n_e(x) = n_0 \mathrm{erfc}\sqrt{\Psi + \left(\frac{x}{2}\right)^2}.$$

This implies that the total number of escaped particles, which we assume come from entirely within some radius r_m, is

$$\begin{aligned} N_e &= 2\pi l_p \int_0^{r_m} n_e(r) r dr \\ &= 2\pi l_p n_0 \int_0^{r_m} \mathrm{erfc}\sqrt{\Psi + \left(\frac{x}{2}\right)^2} r dr \\ &= 8\pi^2 \epsilon_0 l_p n_0 \lambda_d^2 \int_0^{x_m} \mathrm{erfc}\sqrt{\Psi + \left(\frac{x}{2}\right)^2} x dx. \end{aligned} \tag{3.8}$$

We can condense this a bit by defining the function

$$\eta \equiv \int_0^{x_m} \mathrm{erfc}\sqrt{\Psi + \left(\frac{x}{2}\right)^2} x dx. \tag{3.9}$$

η is, necessarily, a numeric function which encapsulates all of the calculations required to determine the amount of escaped charge, in terms of parameters of the initial

plasma. It is a function, instead of a single value, as we have not yet set the value of $\Psi(0)$ and, thereby, $\Psi(x)$. So, our expression becomes

$$N_e = 8\pi^2 \epsilon_0 l_p n_0 \lambda_d^2 \eta(\Psi(0)). \tag{3.10}$$

If we substitute this back into our expression for $\Phi_e(r_m)$, we get

$$\begin{aligned} \Phi_e(r_m) &= 4\pi q n_0 \lambda_d^2 \eta(\Psi(0)) \ln\left(\frac{R_w}{r_m}\right) \\ &= \frac{k_B T}{q} \eta(\Psi(0)) \ln\left(\frac{R_w}{r_m}\right) \\ \Psi(r_m) &= \frac{q}{k_B T}\left(V_b - \Phi_0(0)\right) + \eta(\Psi(0)) \ln\left(\frac{R_w}{r_m}\right). \end{aligned} \tag{3.11}$$

Now, if we provide values of V_b, $\Phi_0(0)$, l_p, n_0, R_w, and T; we can combine Equations 3.7, 3.9, 3.10, and 3.11 to numerically calculate the total escaped charge. By varying V_b at a fixed value of the other parameters, we can produce a curve of escaped charge as a function of blocking potential. In theory, we know or can measure $\Phi_0(0)$, l_p, n_0, and R_w ahead of time. In this case, we have a family of curves determined by their one remaining free parameter, T, and can fit to match data using regression. Even if we don't have this information we can, in practice still generate families of curves and fit for any unknown parameters.

In Figure 3.1, we present a selection of such curves for a variety of possible plasma temperatures. Note that the number of charges usable in the diagnostic and the voltage range over which they emerge are both proportional to the temperature. Adjustments in the space charge of the plasma shift the curves along the voltage axis. Adjustments to the plasma length provide a simple multiplicative scaling of the curve. Finally, adjustments to the plasma density alter the character of the curves' deviation from perfect exponentials. The wall radius cannot be changed, so we generally do not bother fitting for it or allowing it to vary.

3.4 Multi-Species Plasmas

The temperature diagnostic was derived for the case of a single-species plasma. However, in order to create antihydrogen, we must mix positrons and antiprotons. In order to cool the antiprotons, we mix them with electrons. It may be helpful to consider if we can still properly diagnose the temperature of a plasma containing more than one species of particle.

First, we should consider the different methods available for detecting leptons and baryons. We typically count antiprotons leaving the trap by detecting their annihilation on the confinement chamber. This method is not available for counting our leptons as electrons do not annihilate on the wall and we lack efficient gamma ray detectors for observing positron annihilations. We count leptons by extracting them to either our MCP assembly or our Faraday cup. This method is also available for antiprotons.

The MCP response to an antiproton is typically several hundred times greater than for a lepton [10]. Thus, if we have comparable numbers of leptons and antiprotons

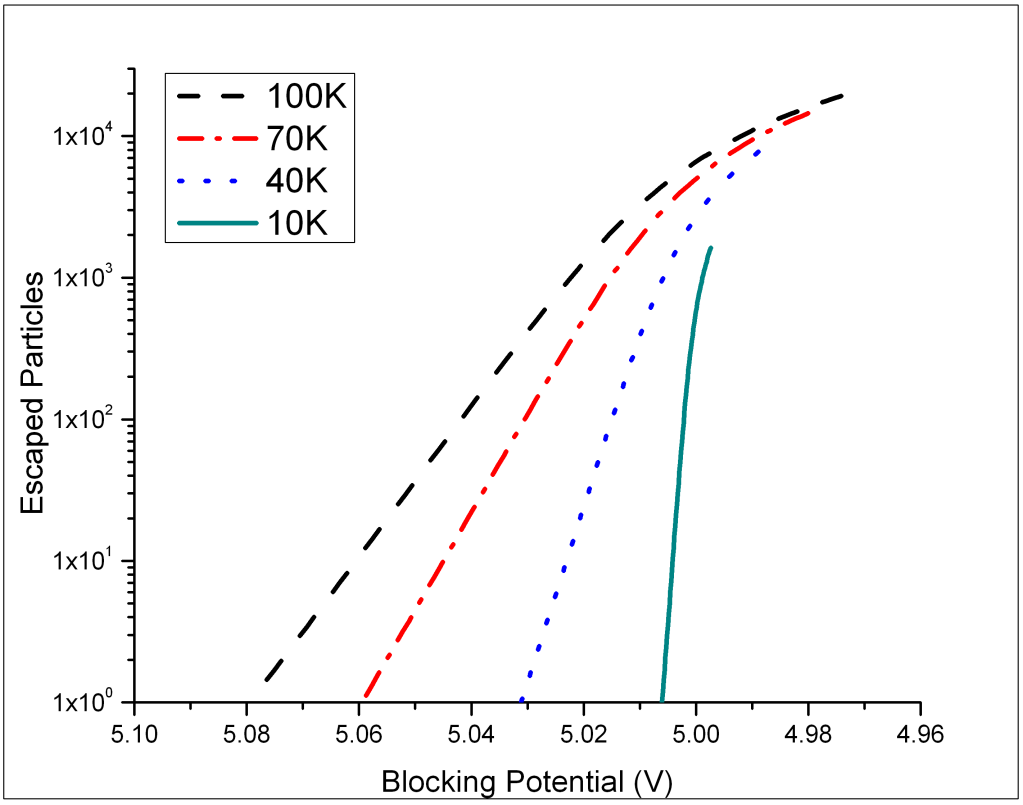

Figure 3.1: Escaping charge as a function of well depth where we have corrected for the plasma's changing space charge, as particles escape. Such curves can be rapidly generated and used to fit experimental data.

and extract them both at the same time, the signal of the antiprotons on the MCP will completely dominate the measurement. On the other hand, we often have many orders of magnitude more leptons than antiprotons. In this case, the signal on the MCP will be dominated by the leptons. In short, it is likely that the MCP will only be able to analyze one of the two species in the trap. Though, so long as we're willing to assume that the two species are in thermal equilibrium, we only need to determine the temperature of one of them.

Of course, this consideration only applies if the two species have the same sign of charge, as oppositely charged species will not be extracted to the same location by the same potential manipulations.

If we have a plasma of two species with the same charge, we might expect that they would arrange themselves in the same spatial configuration, with the ratio of the densities of the two species anywhere in the plasma a constant equal to the ratio of the total number of both particles.

We can consider the two cases of our multi-species plasma and an otherwise identical single-species plasma, with the same charge density distribution and temperature. As we extract particles from either plasma, we should see the same total charge escape, so long as we are within a region in parameter space where the temperature diagnostic is valid for both species. However, as none of our detection methods treat the various particle species identically, the measured charge will change, resulting in a measured charge that is merely proportional to that for the single species plasma. Thankfully, this will have no impact at all on the high-temperature diagnostic and is trivially correctable for the low-temperature diagnostic.

An additional consideration is introduced by the specific geometry of our experiment. The plasmas are usually located over a meter from the MCP. If the two species have a significant mass difference, as in the case of antiprotons and electrons, one species may have a significantly longer travel time to the MCP.

Consider two species with particle masses m_1 and m_2. If the combined plasma was in thermal equilibrium, the two species should have the same temperature and the same average kinetic energy parallel to the magnetic field. We want to compare the travel times of these two species, τ, over some travel distance l_t.

$$\begin{aligned} \frac{1}{2}m_1 v_1^2 = \frac{1}{2}m_2 v_2^2 = E_K \\ \tau_2 - \tau_1 = l_t\left(\frac{1}{v_2} - \frac{1}{v_1}\right) \\ \tau_2 - \tau_1 = l_t\sqrt{\frac{m_1}{2E_K}}\left(\sqrt{\frac{m_2}{m_1}} - 1\right). \end{aligned}$$

If electrons and antiprotons are extracted from our trap at an energy of 10 eV, as is typical, the antiprotons will take, roughly, 22 μs longer to reach the MCP. This is, unfortunately, above our usual resolution of 1-10 μs.

However, if we're in the domain where the high-temperature diagnostic is applicable, the signals on the MCP from both species should be exponentials with the same damping but differing amplitudes, based on the relative densities of the two species and

their gains on the MCP. Adding a time-delay to a pure exponential is equivalent to changing its amplitude and leaving its damping unchanged. Thus, even if the variable travel time of particle species is significant over the course of a measurement, it should not hinder the high temperature diagnostic.

3.4.1 Radial Separation

However, the two species will not necessarily arrange themselves identically in space [18]. If the two species have different charge to mass ratios, they will require differing centripetal forces to keep the particles in their expected ExB rotation. This can lead to radial separation of the plasma components, as in a centrifuge. The heavier species will move outward and the lighter species will move inward.

We can anticipate the magnitude of this effect by comparing the difference in the energy scale of the circular motion of the two particles in the unseparated plasma, $\frac{1}{2}|m_1 - m_2| r_p^2 \omega^2$, to their thermal energy scale, $k_B T$. Here ω is, once again, the angular rotation rate of the plasma.

If the thermal energy is much greater, the plasma will largely remain uniformly mixed. If not, separation may occur, though the precise nature of this will depend on the Debye lengths of the separated plasmas.

In the event that full, strong radial separation occurs and the heavier particles are essentially depopulated within several Debye lengths of the center of the plasma, the techniques presented here are no longer able to reliably determine the temperature of those particles. During extraction for measurement, particles are always extracted preferentially from on the axis, where the space charge is highest and the confining potentials are lowest. Thus, before our diagnostic will be able to sample the heavier particles on the outer edge of the plasma, we will first have to remove most of the lighter particles. The high-temperature diagnostic assumes the plasma space charge is not changed, which is clearly invalidated by this requirement. The low-temperature diagnostic is also invalidated as it explicitly assumes that all measured charge escapes from within a few Debye lengths of the axis.

Radial separation is a symptom of the plasma reaching thermal equilibrium. Thus, in the case of strong separation, we could simply measure the temperature of the lighter particles to determine the temperature of the heavier particles. Thankfully, our capacity to do the former is largely intact. We would expect the density profile of the lighter species to change in a fully separated plasma. However, the high-temperature diagnostic is not sensitive to the specifics of the density profile and should be unaffected.

The low-temperature diagnostic is sensitive to the density profile, in that it assumes a constant density out to a radius of several Debye lengths. This criteria is automatically met if the plasma density is a maximum in the center and the plasma is large enough compared to its Debye length. If the unseparated plasma met this criteria, then the separated plasma should as well, provided the space charge of the original plasma wasn't dominated by the heavier particles. Thus, we should most likely be able to apply the low-temperature diagnostic with only a minimal correction for the particles' increased density.

The intermediate regime, where the density profile of the heavier particles is not a monotonically decreasing function of radius, but is still appreciable within several Debye lengths of the center of the trap, can be rather complicated.

Making a temperature measurement, either on the MCP or with the particle detectors, can be rather problematic as the effective gain, determined by the ratio of the two species in the plasma, changes with radius. Thus, we can no longer necessarily map observed signal with the number of particles escaped from the well.

This completely breaks the assumption underlying the low-temperature diagnostic. However, the high temperature diagnostic is sensitive to neither the radial density distribution nor any radial variation in the gain, so long as the gain is not a function of the blocking potential and the signal remains linearly proportional to the escaped charge, as it should.

Recall that, in Equation 3.2, we expressed the total number of escaped charges as an integral over all radii for which charge can escape and be measured:

$$N_e = 2\pi l_p \int_0^R n(r) \cdot \mathrm{erfc}(\gamma) \cdot r\, dr. \tag{3.12}$$

However, if we take a step back, we can consider applying the temperature diagnostic to charge escaping only from a particular radius, even though we are unable to measure such charges to the exclusion of others. We can also introduce a term, g(r) representing the radially varying average gain of the escaping charge on the MCP due to the partial radial separation of our particle species.

$$dN_e(r) = 2\pi\, r\, dr\, l_p\, n(r)\, g(r) \mathrm{erfc}(\gamma). \tag{3.13}$$

Then, we can follow an analogous procedure to that used for the derivation of the high-temperature diagnostic, provided that the none of the density of the plasma, its space charge, it length, or its effective gain on the MCP are functions of the blocking potential, V_b.

$$\begin{aligned} \frac{\partial}{\partial V_b} \ln(dN_e(r)) &= \left(\frac{\partial}{\partial V_b} \mathrm{erfc}(\gamma) \right) / \mathrm{erfc}(\gamma) \\ &\approx -2\gamma \frac{\partial \gamma}{\partial V_b} = -\frac{q}{k_B T}. \end{aligned}$$

So we see that, as long as the assumptions that originally underpinned the high-temperature diagnostic hold, the signal on the MCP from charge escaping at any particular radius should also be an approximate exponential, with a growth rate given by the plasma temperature. Thus, the high temperature diagnostic should not be compromised by a radially varying gain caused by radial separation of particle species, so long as such separation doesn't contradict any of its underlying assumptions.

There are two cases where the radial variation in gain is less of a concern. If the signal on the MCP of the unseparated plasma was dominated by the leptons, it will still be dominated by leptons after partial separation and concerns about varying gain vanish. Secondly if the scale of the density variations in the separated plasma are much larger than the Debye length, we can approximate both particles' density distributions as constant out to the small radius sampled by the diagnostic. Thus, the effective gain will not observably vary, allowing us to use the high-temperature diagnostic. Of course, not

necessarily knowing what that gain is, even if it is constant, will make the low-temperature diagnostic still somewhat suspect.

If we know the degree of radial separation, we can correct for the radially varying gain, if necessary. Unfortunately, determining the extent of radial separation is, itself, a temperature measurement [19]. However, if one were quite confidant in their knowledge of the other plasma parameters, one could construct a mapping from observed temperature to expected radial separation and then back to real temperature.

3.4.2 Experimental Complications

So, we can see that, while the low-temperature diagnostic may be compromised, the high-temperature diagnostic should, theoretically, be as applicable as ever to multiple-species plasmas, so long as those species produce a linear signal on the MCP. However, in practice, such a situation may reduce the precision of the measurement.

For example, consider a plasma cold enough that the high-temperature diagnostic can only be applied to the first hundred charges to escape. If those charges are all electrons, we would expect, based on numerical simulations, that the temperature measurement will have a standard deviation of roughly 10%, due entirely to statistical variation in the number of escaping charges.

However, if one of those charges, on average, is an antiproton, then the total signal on the MCP from electrons and antiprotons will be comparable. This nearly doubles the standard deviation of temperature measurements.

If 10 of those charges, on average, are antiprotons, then the antiproton signal dominates the electron signal on the MCP. In this case, we're essentially trying to measure the temperature with only 10 particles in our sample. The two cases of, on average, 90 electrons and 10 antiprotons compared to 10 electrons both result in standard deviations of roughly 30%.

Thus, the precision of the high-temperature can be compromised once the signal on the MCP of multiple species of particles with differing gains are comparable, or if whichever species that produces the greater net signal on the MCP is represented in much lower numbers. However, in none of these cases does the average temperature measurement become inconsistent with the true temperature.

3.5 Finite-Length Corrections

3.5.1 Adiabatic Expansion

As stated earlier, the length of the plasma undergoing the diagnostic will necessarily increase during, and almost certainly increase before, the diagnostic process. As the validity of the temperature diagnostic requires this to occur slowly compared to a bounce time for the plasma, it will necessarily be an adiabatic process. This means that the second adiabatic invariant, also known as the bounce invariant $J = \frac{1}{2}\int v_{||} \cdot ds$, will be conserved [20]. Thus, the temperature of the plasma parallel to the magnetic field, which we're trying to measure, will be decreased by our measurement.

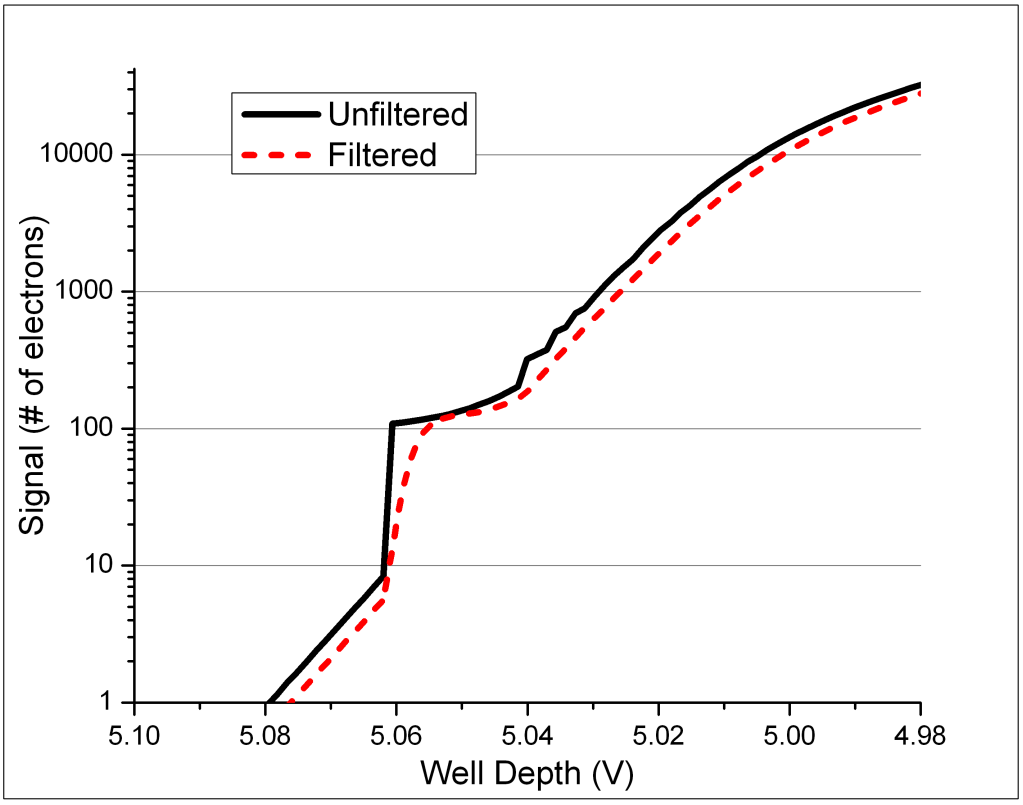

Figure 3.2: Expected charge signal for a multi-species plasma: antiprotons and electrons in a 1:100 mix. The black curve represents one possible charge signal from a temperature measurement of such a plasma, selected for the early emergence of an antiproton. Note that the plasma temperature is still measurable, so long as we can measure using at least the first 1000 emerging particles. The red curve represents the same signal run through a 300Hz - 100kHz bandpass filter, as is the case for data taken on the ALPHA apparatus.

By simple dimensional analysis, we can see that, when the kinetic energy of the plasma is changing with its length to preserve the second adiabatic invariant, $\frac{\delta E}{\delta l} = -2\frac{E}{l}$. Thus, if we know how the length of the plasma varies over time, we can also determine its kinetic energy, though we may need to resort to numerical methods.

Unfortunately, it is not necessarily trivial to determine the length of a given plasma as a function of time. However, we do have, as a starting point, the knowledge of the well depth when charge first begins to escape from the well and the well depth as a function of time, as we require this information to properly apply the temperature diagnostic in the first place.

In order to determine, even roughly, how the length of the plasma changes as the applied vacuum potentials change, we need to also know the space charge of the plasma, as will be explained shortly. We can, in theory, determine this based on the measured temperature of the plasma and the afore-mentioned well depth of first escape. However, this requires us to recalculate the correction for every measurement, or at least every new variety of plasma used in a given well. It would be much simpler if we could calculate a correction based solely on the well depth of first escape and the details of the potential manipulations, allowing us to develop a single chart applicable to all measurements in a given well. We can do this, if we consider two limiting cases.

First, we consider an ensemble of particles with a negligible space charge compared to their kinetic energy; that is, essentially free particles. With no space charge, the bounce length for a particle in a given well is determined by its kinetic energy. Thus, J becomes an easily calculated, monotonic function of the particles' depth in the well.

As an illustrative example, consider the piecewise harmonic well with $U = \frac{1}{2}kz^2$, for $|z| \leq l_t$ and zero elsewhere, where k is a parameter representing the depth of the well and l_t is the length of the well. Of course, this is a manifestly non-physical well, but there are no physical wells that will suffice for a simple analytical treatment.

By conservation of energy, we have that $\frac{1}{2}mv^2 = \frac{1}{2}mv_0^2 - \frac{1}{2}kz^2$, where v_0 is the velocity of the particles in the center of the well. Thus, the bounce length for a particle, l, will be set by $\frac{1}{2}mv_0^2 = \frac{1}{2}k\left(\frac{l}{2}\right)^2$. Finally, utilizing the symmetry of the well, we can calculate

$$\begin{aligned} J = 2\int_0^{l/2} v dz &= 2v_0 \int_0^{l/2} \sqrt{1 - \left(\frac{2}{l}\right)^2 z^2} dz \\ &= \frac{\pi}{4} v_0 l = \frac{\pi}{2}\sqrt{\frac{m}{k}} v_0^2 = \sqrt{\frac{\pi^2}{mk}} E_k. \end{aligned}$$

So, as the well becomes more shallow and k decreases, the kinetic energy, and thereby the temperature, of the particles will decrease as the square root of k.

At the opposite extreme, we consider a plasma with a low enough temperature that the space charge of the plasma completely flattens the well and the Debye length of the plasma is much shorter than the plasma length. In this case, the bounce length of a particle is equal to the length of the plasma. This makes the adiabatic invariant trivial to calculate. $J = vl_p$.

Unfortunately, there is the added complication of determining the length of the plasma. In this low-temperature limit, particles begin to escape when the depth of the well

is equal to the space charge of the plasma. If we can determine how the space charge of the plasma changes as the well changes shape, we can find the length of the plasma.

The simplest possible assumption is that the space charge of the plasma does not change. This is, of course, only approximately correct, and only for small changes in the shape of the well. It does, however, make determining the change in the length of the plasma a simple matter of consulting the applied potentials.

To return to the example of the infinite harmonic well, this approximation would immediately yield $\frac{1}{2}k\left(\frac{l_p}{2}\right)^2 = \Phi$. Here, Φ is the change in the on-axis potential of the plasma from one end to the longitudinal center of the plasma. So, we can easily calculate

$$J = vl_p = \sqrt{\frac{2E_k}{m}}\sqrt{\frac{8\Phi}{k}}$$
$$J^2 = \frac{16\Phi}{m}\frac{E_k}{k}.$$

So, in this limit, the temperature of the plasma will decrease linearly with k, as opposed to as $\sqrt{k}$.

Of course, the space charge of the plasma will most likely change. Unfortunately, there is not a definite way to determine the degree of this change without lengthy and somewhat difficult calculations. However, if we assume that the radius of the plasma does not change significantly, then the integral of the space charge over the length of the plasma will be conserved, as it will be in approximately constant proportion to the total number of particles. $\int_{-l/2}^{l/2}\Phi dx = AN$.

Applying this constant particle number approximation to the infinite harmonic well yields $AN = \frac{4}{3}k\left(\frac{l}{2}\right)^3$. Thus, knowing the length of the plasma when it escapes the well, we can find its length at any earlier time. Applying this to the conservation of the adiabatic invariant yields

$$J^2 = v^2l^2 = \frac{2}{m}\left(\frac{6AN}{k}\right)^{2/3}E_k.$$

Thus, in this limit, the temperature of the plasma decreases as $k^{2/3}$, intermediate between the limit of the free particles and the assumption of an unchanging plasma space charge.

Now, it remains to relate the change in kinetic energy parallel to the magnetic field to a change in the plasma temperature parallel to the magnetic field. The obvious answer is that they're linearly related by a factor of half Boltzmann's constant. However, we have to consider coupling to the transverse temperature of the plasma. It is, as stated above, an assumption of the temperature diagnostic that the diagnostic occurs over a time short compared to a collision time, but this restriction doesn't necessarily apply to manipulations made before the diagnostic, which this correction is also intended to address. Regardless, even in the event of full equilibrium between the longitudinal and transverse temperature, the only change is that 2/3 of the energy reduction caused by the adiabatic expansion cools the transverse temperature instead. Of course, this consideration is irrelevant in the case of the single-particle limit, as collisions should be sufficiently suppressed in said limit to make equilibration much slower and, therefore, negligible.

Using these various models and a set of potentials for a given measurement, it is possible to construct a set of simple curves giving the expected correction to the measured temperature, based on the voltage at which charge begins to escape the well.

3.5.2 Change in Space Charge

As we just discussed, the space charge of the plasma will necessarily decrease as the length of the well increases during and preceding the diagnostic. However, when deriving Equation 3.4, we assumed that the derivative of the space charge with respect to the blocking voltage was zero. If we remove this assumption, Equation 3.4 becomes

$$\frac{\partial}{\partial V_b} \ln(N_e) = -\frac{q}{k_B T} \left(1 - \frac{\partial \Phi}{\partial V_b}\right). \tag{3.14}$$

Thus, this effect will reduce the right-hand side of the equation and cause the temperature to appear higher than it actually is.

For a given potential configuration, it is possible to calculate $\frac{\partial \Phi}{\partial V_b}$ as a function of Φ and V_b. For example, in the case of our infinite harmonic well, $\frac{\partial \Phi}{\partial V_b} = \frac{1}{3}\frac{\Phi}{V_b}$. In general, the factor of 1/3 will be replaced with a numeric function, $a(V_b)$. Unfortunately, even after calculating the correction for a particular well, one needs to know both the blocking potential and the space charge to determine the shift in temperature; unless, in analogy with the correction due to adiabatic expansion, we make assumptions regarding the relationship between the space charge and blocking potential.

In the high temperature, single-particle limit, the space charge of the plasma is negligible. Thus, any change in the space charge is also negligible and this correction vanishes.

In the limit of the zero-temperature plasma, no charge escapes from the well until the blocking potential is equal to the space charge of the plasma. In this case, the relationship between the measured, T_m, and real, T_f, temperatures is $T_f = T_m\,(1 - a(V_b))$.

Unfortunately, these bounds are not terribly constraining, as $a(V_b)$ is generally on the order of 1/2, which corresponds to a 100% difference between the two limiting cases.

This correction, in combination with the previous correction for adiabatic expansion, can be used to construct curves giving the expected error in a temperature measurement as a function of when charge begins to escape the well, during the extraction process. An example, for our perfectly harmonic well, is depicted in Figure X. While the example well is manifestly non-physical, the result is generally representative of curves constructed for physically realizable wells used in actual experiments. Even if one doubts the veracity of any of the possible models represented, the true behavior of the plasma is almost certainly intermediate between them, with the corresponding correction lying somewhere in the range depicted.

3.6 Comparisons to Simulation

Of course, a diagnostic is only as good as the measurements it produces. So, we decided to compare the results of the diagnostic to the results produced by numerical simulations [21].

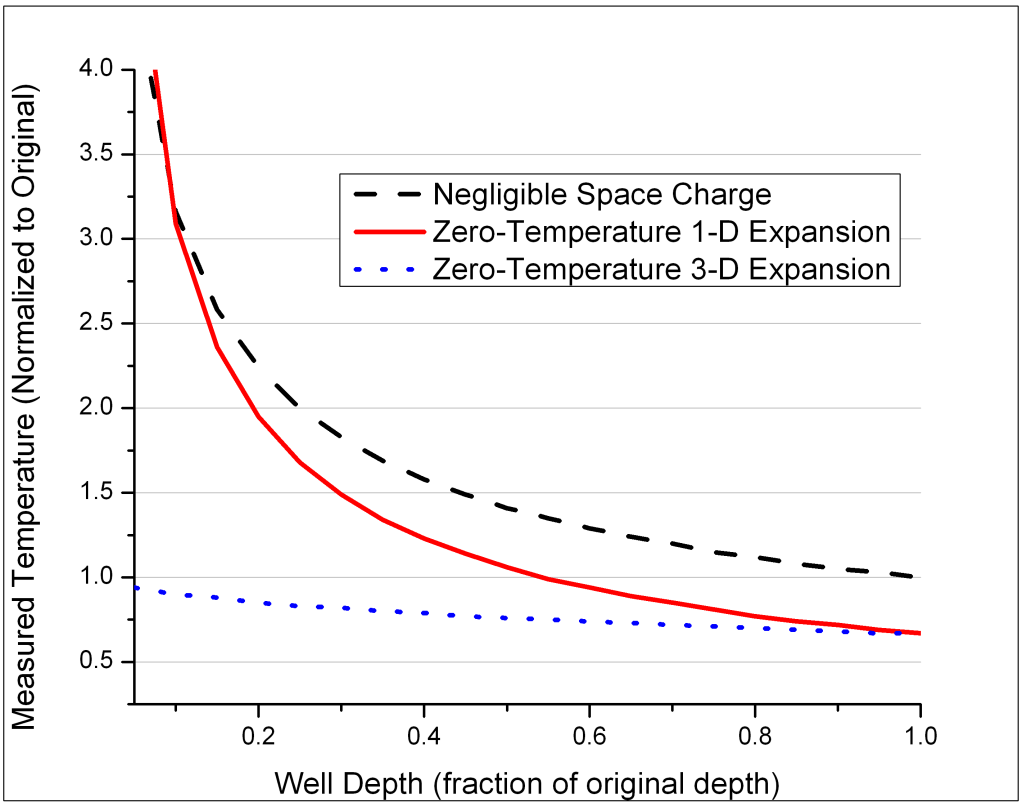

Figure 3.3: Correction curve for hypothetical temperature measurements: similar curves can be constructed numerically for real temperature measurements. This allows us to estimate the error in our measurements based on the plasmas measured temperature and space charge. For plasmas far from any of these limiting cases or of particular importance to us, we can instead resort to particle-in-cell simulations specific to certain sets of plasma parameters.

The simulations were done with a two-dimensional particle-in-cell code with the assumption of global thermal equilibrium. Additional simulations were done for the case of thermal equilibrium only along field lines, but the results were qualitatively similar.

In the simulation, a plasma with a specified number of particles, density, and temperature would be placed in a specified well. Then, the well would undergo the same alterations as during the temperature diagnostic. The number of charges escaping from the well were recorded and the temperature diagnostic was applied to them, exactly as for real data.

The well in question, for the case being considered here, was the well in which positrons were held prior to mixing. This well consisted on only a single electrode (approximately 1 cm long). Thus, we would expect errors due to the finite length of the plasma to, potentially, be quite important.

The results are shown in Figure 3.3. We present the percentage error in the measured temperature both before and after correction for the finite length errors discussed in the previous section.

We note that, for this particular case, the error due to the changing space charge of the plasma is generally more significant than that due to adiabatic cooling, resulting in the measured temperature almost always being higher than the original temperature of the plasma. The effect becomes more pronounced as the plasma becomes colder and denser, or as the potential energy of the plasma becomes larger, in comparison to its thermal energy. Fortunately, by applying the corrections described in the previous section, we are able to determine the temperature of these simulated plasmas to within 20% in most cases, implying that we can do the same for the real plasmas we wish to diagnose.

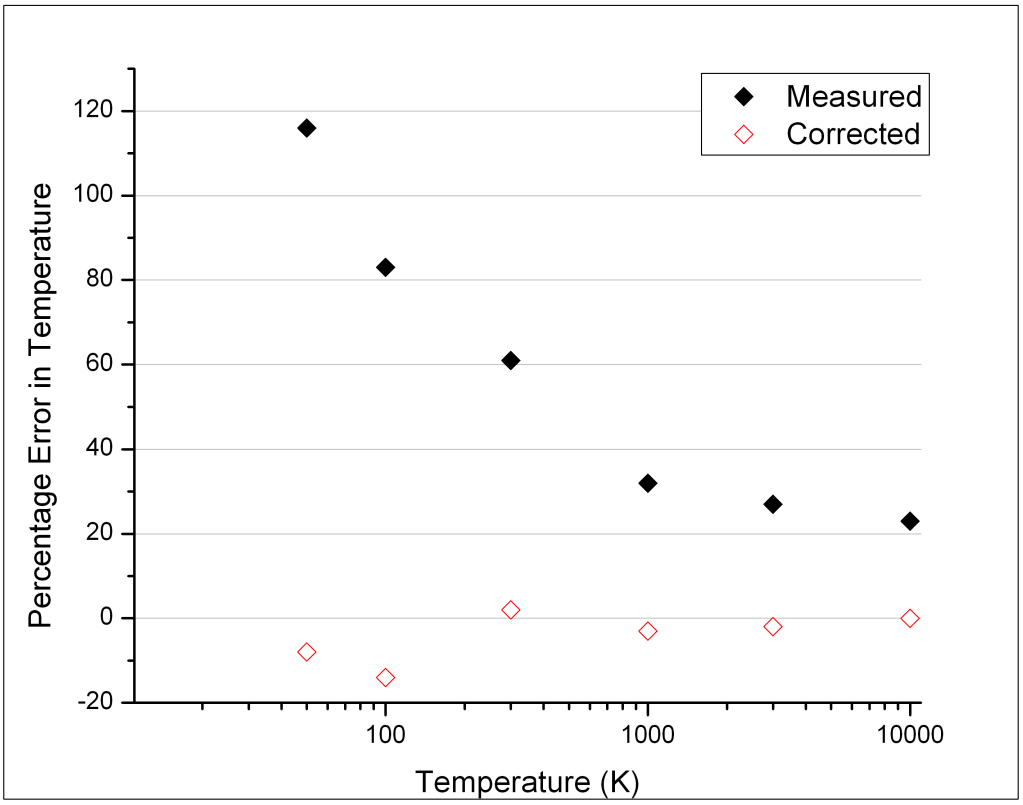

Figure 3.4: Expected errors and corrections for temperature diagnostic: all data points represent the results of particle-in-cell simulations of a single, particular temperature measurement while the initial equilibrium temperature of the plasma is varied, either with or without the finite-length corrections discussed.

Chapter 4

Diffusion and Heating

Having established the applicability and principles of our temperature diagnostic, we now establish a model for one particular effect we used the diagnostic to observe and characterize.

We will determine the heating of an expanding non-neutral plasma. In particular, we will focus on expansion due to diffusion, in several different regimes of applicability.

Then, we will develop a model for the enhancement to diffusion caused by immersing our plasmas in a multipole field and combine this with the previous work to attempt to predict the temperature of a plasma undergoing such diffusion.

4.1 Self-heating of a Diffusing Plasma

We assume that a plasma will diffuse according to the classical diffusion equation:

$$\frac{\partial n}{\partial t} = \nabla \bullet (D \nabla n). \tag{4.1}$$

where n is the density of the plasma and D, to be determined, is the particle radial diffusion coefficient.

If the plasma is azimuthally and longitudinally symmetric and the diffusion coefficient has a simple power-dependence on the radial coordinate: $D = D_0 r^p$, then the diffusion equation simplifies to

$$\frac{\partial n}{\partial t} = \frac{D(r)}{r}\left((p+1)\frac{\partial n}{\partial r} + r\frac{\partial^2 n}{\partial r^2}\right). \tag{4.2}$$

The plasma has an electrostatic self-energy associated with its electric Field, E(r, t):

$$U(t) = \frac{\epsilon_0}{2}\int_V E^2 dV. \tag{4.3}$$

If we assume the plasma is azimuthally and longitudinally symmetric, then we need only concern ourselves with the electrostatic self-energy per unit length. Under this approximation, we can write the electric field of the plasma:

$$E(r,t) = \frac{q}{2\pi\epsilon_0}\frac{1}{r}\int_0^r 2\pi x n(x) dx. \tag{4.4}$$

As the plasma diffuses, the electrostatic self-energy will decrease, as the electric field does positive work on the charges moving outward. This work will increase the kinetic energy of the particles. Assuming that collisions among the particles occur at a rate significantly faster than the diffusion, this will result in an increase in the plasma temperature.

The heat capacity of the plasma per unit length should be merely the heat capacity of a single charge, $\frac{3}{2}k_B$ times the number of charges per unit length, λ .

$$\begin{aligned}\frac{\partial T}{\partial t} &= \frac{2}{3k_B\lambda}\frac{\partial U}{\partial t} \qquad (4.5)\\ &= \frac{\epsilon_0}{3k_B\lambda}\int_V \frac{\partial E^2}{\partial t}dV\\ &= \frac{2\epsilon_0}{3k_B\lambda}\int_V E\frac{\partial E}{\partial t}dV\\ &= \frac{4\pi q^2}{3k_B\lambda\epsilon_0}\int\left(\frac{1}{s}\int_0^s nrdr\right)\left(\frac{1}{s}\int_0^s \frac{\partial n}{\partial t}rdr\right)sds. \qquad (4.6)\end{aligned}$$

Thus, in theory, if we know the diffusion coefficient and the plasma distribution at any given time, we can determine the instantaneous diffusion based heating. If the diffusion coefficient is time-invariant, then we can also, theoretically, determine this heating at any later time.

4.2 Solutions to the Diffusion Equation

In practice, knowing both the diffusion coefficient and the initial plasma distribution is not sufficient to easily determine the plasma distribution at any later time, especially if the diffusion coefficient itself varies in time or space. Thus, we consider a number of possible approximations to simplify the task.

4.2.1 Free Uniform Diffusion

First, we want to select as simple an initial plasma distribution as possible. Any distribution will be described in terms of its linear charge density λ. The simplest possible distributions will depend on only one time-varying parameter.

The first such distribution to come to mind is the flat-topped plasma distribution, with uniform density within some radius. While this distribution is, potentially, a reasonable approximation to a physical distribution, it also results in non-continuous derivatives. Thus, it is rather problematic to use when solving a differential equation.

One distribution that retains the desired compactness of the flat-topped distribution with continuous derivatives and is still described by only one spatial parameter is the Gaussian:

$$n(r) = \frac{\lambda}{\pi r_p^2}e^{-(r/r_p)^2}. \qquad (4.7)$$

Of course, the same could be said for analogous functions involving other powers of the radius than two. However, the Gaussian has the useful property of being a potential

solution to our diffusion equation. Plugging it in to Equation 4.2 yields

$$n\frac{\partial r_p}{\partial t}\frac{2}{r_p}\left(\frac{r^2}{r_p^2}-1\right)=nD\frac{4}{r_p^2}\left(\frac{r^2}{r_p^2}-1-\frac{p}{2}\right).$$

Unfortunately, this only has a solution when p=0; that is, when the diffusion coefficient is spatially uniform. In that case, the result further simplifies to give us

$$\begin{aligned} D &= \frac{r_p}{2}\frac{\partial r_p}{\partial t} \\ \frac{\partial n}{\partial t} &= nD\frac{4}{r_p^2}\left(\frac{r^2}{r_p^2}-1\right). \end{aligned} \tag{4.8}$$

If we consider this result, we see that it predicts that the density will decrease at radii less than r_p, the root mean square radius of the distribution, and increase at larger radii. This is entirely in keeping with the idea of a spatially concentrated distribution diffusing to larger radii.

If we know how the diffusion coefficient varies with time and the size of the plasma, we can use Equation 4.8 to determine the size of the plasma as a function of time. For example, if the diffusion coefficient varies with neither parameter, the size of the plasma will increase as the square root of elapsed time, as one might expect for a diffusive process.

Now, we can directly evaluate the heating of the plasma over time:

$$\begin{aligned} \frac{\partial T}{\partial t} &= \frac{16\lambda q^2}{3\pi k_B\epsilon_0}\frac{D}{r_p^6}\int\frac{1}{s}\left(\int_0^s re^{-\frac{r^2}{r_p^2}}dr\right)\left(\int_0^s r\left(\frac{r^2}{r_p^2}-1\right)e^{-\frac{r^2}{r_p^2}}dr\right)ds \\ &= \frac{4\lambda q^2}{3\pi k_B\epsilon_0}\frac{D}{r_p^2}\int\frac{1}{s}\left(\frac{s^2}{r_p^2}e^{-\frac{s^2}{r_p^2}}\right)\left(1-e^{-\frac{s^2}{r_p^2}}\right)ds \\ &= \frac{\lambda q^2}{3\pi k_B\epsilon_0}\frac{D}{r_p^2}. \end{aligned} \tag{4.9}$$

One may wish to note that $\frac{\lambda}{r_p^2}$ is proportional to the average density of the plasma. Thus, the rate of change of the plasma's thermal energy is directly proportional to the product of the diffusion coefficient and the plasma's average density.

There are several important caveats to this particular result. First off, it is invalid if the diffusion coefficient varies spatially. Secondly, the integrals done to determine the heating were done over all of space. The Gaussian density distribution also results in a non-zero density everywhere in space. Our plasmas are held inside conducting cylinders. Thus, neither the plasma nor its electric field extends beyond some certain radius. However, if the plasma is much smaller than this radius, this result should still be approximately correct.

4.2.2 Bounded Uniform Diffusion

Luckily, we also know of solutions to the diffusion equation, with spatially uniform diffusion coefficient, for the, more physical, bounded case. The eigenfunctions of the diffusion equation, with our actual boundary conditions, are the zeroth-order Bessel functions of the first kind.

It would be convenient if we could approximate our initial plasma distribution as one of these functions. However, all but one of these functions are negative for certain ranges of radii. A negative density is certainly unphysical. The one remaining Bessel function depicts a plasma roughly as large as its confining cylinder and results in large quantities of plasma being lost directly to the wall. While this may be an interesting case to consider in other applications, we are more likely to deal with plasmas that are small compared to their confining cylinders. Thus, we need more generality than a single Bessel functions.

Bessel functions form a complete basis with which we can expand any plasma distribution. Thus, we can express an arbitrary radial distribution as a linear combination of Bessel functions in what is known as a Bessel-Fourier series.

$$n(r,t) = \sum_j A_{\beta_j} e^{-\beta_j^2 Dt/R^2} J_0\left(\frac{\beta_j r}{R}\right),$$

where $J_n(x)$ is the nth-order Bessel function of the first kind, R is the confining radius (where the plasma density is necessarily zero), and β_j represents the jth zero of $J_0(x)$. The coefficients are given by

$$A_{\beta_j} = \frac{2}{R^2 J_1^2(\beta_j)} \int_0^R r n(r) J_0\left(\frac{\beta_j r}{R}\right) dr.$$

With this formulation, we can evaluate the heating of the plasma.

$$\begin{aligned} \frac{1}{s}\int_0^s nr dr &= \sum_j A_{\beta_j} e^{-\beta_j^2 Dt/R^2} \int_0^s J_0\left(\frac{\beta_j r}{R}\right) r dr \\ &= \sum_j A_{\beta_j} e^{-\beta_j^2 Dt/R^2} \left(\frac{R}{\beta_j}\right) J_1\left(\frac{\beta_j s}{R}\right), \end{aligned}$$

by a convenient property of the Bessel functions. Similarly,

$$\frac{1}{s}\int_0^s \frac{\partial n}{\partial t} r dr = \sum_j A_{\beta_j} \left(\frac{-\beta_j^2 D}{R^2}\right) e^{-\beta_j^2 Dt/R^2} \left(\frac{R}{\beta_j}\right) J_1\left(\frac{\beta_j s}{R}\right).$$

Combining these,

$$\frac{\partial T}{\partial t} = -\frac{4\pi q^2}{3k_B \lambda \epsilon_0} \sum_i \sum_j A_{\beta_i} A_{\beta_j} D \left(\frac{\beta_j}{\beta_i}\right) e^{-(\beta_j^2+\beta_i^2)Dt/R^2} \int_0^R J_1\left(\frac{\beta_i s}{R}\right) J_1\left(\frac{\beta_j s}{R}\right) s ds.$$

Luckily, Bessel functions are orthogonal, and the integral in the sum is zero unless $\beta_i = \beta_j$.

Thus, we reach our final expression for the change in temperature, without selecting a particular density distribution:

$$\frac{\partial T}{\partial t} = \frac{2\pi q^2}{3k_B \lambda \epsilon_0} \sum_j A_{\beta_j}^2 R^2 D e^{-2\beta_j^2 Dt/R^2} J_1^2(\beta_j).$$

Now consider the simplest physically-possible case, where the Bessel-Fourier expansion consists of a single term; the first. In this case, $A_{\beta_1} = n(0) \approx \lambda/\pi r_p^2$, and we have

$$\begin{aligned}\frac{\partial T}{\partial t} &= \frac{2\pi q^2}{3k_B\lambda\epsilon_0}\left(\frac{\lambda}{\pi r_p^2}\right)^2 R^2 D J_1^2(\beta_1) e^{-2\beta_1^2 Dt/R^2} \\ &= \frac{q^2}{6\pi k_B \epsilon_0} D \frac{\lambda R^2}{r_p^4} e^{-2\beta_1^2 Dt/R^2}.\end{aligned}$$

Note that, in this case, the plasma radius does not vary in time and is a fixed fraction of R. Thus, the time-independent portion of this result actually varies as $1/r_p^2$.

However, as stated earlier, we are particularly interested in plasma density distributions with a radial scale $r_p << R$. The Bessel functions we're using to expand the density, $J_0(\beta r)$, have a global maximum at r = 0 and their first zero at r = β_1/β. Thus, the largest contribution to their integral comes from within this radius and we expect the Bessel-Fourier expansion to be dominated by the terms near $\beta = \frac{\beta_1 R}{r_p}$.

For the case of large argument, one can asymptotically expand the Bessel functions. Specifically,

$$\begin{aligned}J_0(r >> \beta_1) &\approx \sqrt{\frac{2}{\pi r}}\cos\left(r - \frac{\pi}{4}\right) \\ J_1(r >> \beta_1) &\approx \sqrt{\frac{2}{\pi r}}\sin\left(r - \frac{\pi}{4}\right).\end{aligned}$$

Since β_j is defined as a zero of $J_0(r)$, we can see that

$$J_1^2(\beta_j >> \beta_1) \approx \frac{2}{\pi\beta_j}.$$

While this expression may have been derived for large j, it is accurate to within 2% for all j.

Unfortunately, for most reasonably physical density distributions, the coefficients of the Bessel-Fourier expansion must be calculated numerically. One exception is the flat-topped plasma distribution, where $n(r) = \frac{\lambda}{\pi a^2}$ for $r \leq a$ and is zero elsewhere. The flat-topped distribution, unlike the Bessel functions, is not an eigenstate of the diffusion equation. Thus, the plasma distribution can only be exactly flat-topped at a single moment in time. However, we will assume that the plasma stays approximately flat-topped and place all time-dependence of the density distribution in its size, a.

In this case,

$$\begin{aligned}A_{\beta_j} &= \frac{2}{R^2 J_1^2(\beta_j)}\left(\frac{\lambda}{\pi a^2}\right)\int_0^a r J_0\left(\frac{\beta_j r}{R}\right) dr \\ &= \frac{2}{R^2 J_1^2(\beta_j)}\left(\frac{\lambda}{\pi a^2}\right)\left(\frac{aR}{\beta_j}\right) J_1\left(\frac{\beta_j a}{R}\right) \\ &\approx \frac{\lambda}{aR} J_1\left(\frac{\beta_j a}{R}\right).\end{aligned}$$

Knowing the coefficients, we can write

$$\frac{\partial T}{\partial t} \approx \frac{4q^2}{3k_B\epsilon_0}\frac{\lambda}{a^2}D\sum_j e^{-2\beta_j^2 Dt/R^2}\frac{1}{\beta_j}J_1^2\left(\frac{\beta_j a}{R}\right).$$

Note that we've now removed all dimensionful parameters from inside the sum over j.

The zeroes of $J_0(r)$ are approximately evenly spaced by π. As a/R becomes smaller, the number of terms of this sum with a non-negligible contribution to the total increases. If the number of significant terms is large enough, we can approximate the sum with an integral, provided the terms vary slowly, as they do. In practice, if a/R $\leq$ 1/10, as is the case for most of our plasmas, this approximation is good to within a few percent.

$$\begin{aligned}\sum_j \frac{1}{\beta_j}J_1^2\left(\frac{\beta_j a}{R}\right)e^{-2\beta_j^2 Dt/R^2} &\approx \int_0^\infty \frac{1}{\pi x}e^{-2\pi^2 x^2 Dt/R^2}J_1^2\left(\frac{\pi x a}{R}\right)dx \\ &= \frac{1}{2\pi}\left[1-e^{-a^2/4Dt}\left(I_0\left(\frac{a^2}{4Dt}\right)+I_1\left(\frac{a^2}{4Dt}\right)\right)\right] \\ &\equiv \frac{1}{2\pi}\left(1-S\left(\frac{a^2}{4Dt}\right)\right).\end{aligned}$$

Here, $I_n(r)$ is the nth order modified Bessel function of the first kind. They are also known as the hyperbolic Bessel functions, in analogy with the hyperbolic trigonometric functions. S(x) is merely used as a convenient shorthand.

While the function itself is relatively complicated, it can be asymptotically expanded for both large and small arguments:

$$\begin{aligned}S\left(\frac{r_{p0}^2}{2Dt} >> 1\right) &\approx \sqrt{\frac{4Dt}{r_{p0}^2}}\left(1-\frac{Dt}{4r_{p0}^2}\right) \\ S\left(\frac{r_{p0}^2}{2Dt} << 1\right) &\approx 1-\frac{r_{p0}^2}{4Dt}.\end{aligned}$$

So, we can see that the heating of the plasma is an always decreasing function of time, decreasing like $1-\sqrt{t}$ at early times and like 1/t at late times.

We wish to define the plasma radius as the root mean square radius of the plasma distribution. Thus, $a=\sqrt{2}r_{p0}$, where r_{p0} is the RMS plasma radius at t=0. Plugging all of this together yields

$$\frac{\partial T}{\partial t} \approx \frac{q^2}{3\pi k_B\epsilon_0}\frac{\lambda}{r_{p0}^2}D\left(1-S\left(\frac{r_{p0}^2}{2Dt}\right)\right), \tag{4.10}$$

a functional form that should be correct up to a numeric correction for any sufficiently small, physical plasma distribution.

At t=0, this result may look identical to the result for the Gaussian distribution undergoing free diffusion. However, there is the important distinction that, in the prior result, r_p is a function of time, while r_{p0} is not. Thus, the two expressions only agree at t=0.

4.2.3 Time Dependence

Unfortunately, our description for bounded diffusion does not describe the radius of the plasma as a function of time, unlike the unbounded result. It will be useful to determine what the actual time dependence is.

We want to describe the size of the plasma with its root mean square radius:

$$r_p^2 = \left(\int_0^R 2\pi r^3 n(r) dr\right) / \left(\int_0^R 2\pi r n(r) dr\right). \tag{4.11}$$

Of course, the normalizing integral should simply give λ. However, there will be some time dependence corresponding to diffusive loss of particles to the walls. While we are not currently interested in this effect, it is important to make sure we can properly neglect its effect on the size of the plasma.

If we, once again, assume a flat-topped distribution, small compared to the electrode radius, and apply our previous results, we can evaluate the integrals:

$$\begin{aligned}\int_0^R 2\pi r^3 n(r) dr &\approx \frac{2\pi\lambda}{aR}\int_0^R r^3 \sum_j J_1\left(\frac{\beta_j a}{R}\right) J_0\left(\frac{\beta_j r}{R}\right) e^{-\beta_j^2 Dt/R^2} dr \\ &= \frac{2\pi\lambda}{aR}\sum_{\beta_j} J_1\left(\frac{\beta_j a}{R}\right) e^{-\beta_j^2 Dt/R^2}\int_0^R r^3 J_0\left(\frac{\beta_j r}{R}\right) dr,\end{aligned}$$

and similarly for the normalizing integral.

Doing the spatial integrals

$$\begin{aligned}\int_0^R r^3 J_0\left(\frac{\beta_j r}{R}\right) dr &= \frac{R^4}{\beta_j^2}\left(2J_2(\beta_j) - \beta_j J_3(\beta_j)\right) = \frac{R^4}{\beta_j^3} J_1(\beta_j)\left(\beta_j^2 - 4\right) \\ \int_0^R r J_0\left(\frac{\beta_j r}{R}\right) dr &= \frac{R^2}{\beta_j} J_1(\beta),\end{aligned}$$

where we've used the property of the Bessel functions that $J_n(x) = \frac{x}{2n}(J_{n-1}(x) + J_{n+1}(x))$ to rewrite the result of the first integral.

This leaves us with

$$r_p^2 \approx R^2\left(1 - \left(\frac{\sum_j \frac{4J_1(\beta_j)}{\beta_j^3} J_1\left(\frac{\beta_j a}{R}\right) e^{-\beta_j^2 Dt/R^2}}{\sum_j \frac{J_1(\beta_j)}{\beta_j} J_1\left(\frac{\beta_j a}{R}\right) e^{-\beta_j^2 Dt/R^2}}\right)\right).$$

Unfortunately, $J_1(\beta_j)$ reverses sign at each value of j, making it a quickly varying function. This prevents us from being able to approximate these sums as integrals. Fortunately, both sums converge relatively swiftly, allowing us to find a numeric approximation.

If we do this, we find that the room mean square radius of the plasma starts out at $a^2/2$, as we'd expect and, so long as the plasma remains small compared to the electrodes, this radius increases as roughly the square root of time elapsed. Once, the plasma becomes large, its rate of expansion slows as the radius asymptotes to ≈ 0.6 R, the constant value corresponding to only the lowest order Bessel function that the plasma distribution will approach, as particles are lost to the wall.

4.2.4 Numeric Solutions

Unfortunately, it is very difficult to generalize the preceding analysis for the case of a spatially varying diffusion coefficient. However, if we know the density distribution and diffusion coefficient at any particular time, we can numerically determine the instantaneous heating rate.

Consider a density distribution of the form $n(r) = Ae^{-(\frac{r}{r_p})^{\aleph}}$, normalized to the linear particle density, λ, where r_p is the room mean square plasma radius and $\aleph$ is a parameter describing the shape of the distribution: two for a Gaussian, higher for more "flat-topped" distributions, and less (but still greater than one) for broader ones.

We are interested in diffusion caused by the addition of a magnetic multipole of order α to the standard Penning trap. ($\alpha = 2$ for a quadrupole, 4 for a octupole, and so on). Thus, for reasons that will be illustrated later, we expect the diffusion coefficient to vary as $r^{2\alpha-2}$.

Using these two assumptions, we can numerically evaluate the integral in Equation 4.6. The result is $D(r_p)\frac{\lambda^2}{r_p^2}$ times a numerical factor that increases weakly with α and $\aleph$ and does not depend on the radius of the confining electrodes (beyond which the electric field due to the plasma is necessarily zero) so long as the plasma extent is small compared to the electrodes. For example, for the case of a Gaussian distribution in an octupole, the numerical factor is .038, in SI units. We note that this is 50% larger than the equivalent result in Equation 4.9. Thus, for the sake of clarity, we will simply incorporate this correction with a direct modification of that result.

4.3 Finite Length Correction to Heating

The above calculations assume a plasma of infinite length. This is, obviously, not physical and we should consider how this deviation from our model might affect the results.

The simplest approach is to directly compare the two limiting cases: an infinite cylinder and a sphere.

For a uniform sphere of radius a containing N elementary charges, the total electrostatic energy is given by

$$U_s = \frac{3}{5}\frac{q^2}{4\pi\epsilon_0}\frac{N^2}{a}.$$

For a uniform cylinder of radius a and length l (which we will take as infinite) containing λ elementary charges per unit length, contained within an infinite cylindrical conducting wall of radius R (to prevent the divergence of the electrostatic energy), the total electrostatic energy is given by

$$U_c = \frac{q^2}{4\pi\epsilon_0}\lambda^2 l\left(\frac{1}{4} + \ln\left(\frac{R}{a}\right)\right).$$

A direct comparison of these two is not terribly illuminating, even if we ignore the fact that our two charge distributions exist in different environments. However, we are only

actually interested in how the electrostatic energy of these distributions changes as they expand.

If we take the derivatives of these expressions with respect to radius and, additionally, rephrase the expression for the sphere to include $\lambda = N/2a$, we get

$$\begin{aligned}\frac{\delta U_s}{\delta a} &= -\frac{12}{5}\frac{q^2\lambda^2}{4\pi\epsilon_0} \\ \frac{\delta U_c}{\delta a} &= -\frac{q^2\lambda^2}{4\pi\epsilon_0}\frac{l}{a} \\ \frac{\delta U_c}{\delta a} &= \frac{5}{12}\frac{l}{a}\frac{\delta U_s}{\delta a}.\end{aligned}$$

From this, it is tempting to conclude that the rate of change of electrostatic energy for a finite cylinder will be equal to that of a sphere, multiplied by the cylinders aspect ratio and a numeric factor between 1 and 5/12.

Unfortunately, it is not possible to analytically calculate a similar result for an arbitrary finite cylinder. However, numeric calculations fully support this result. For example, a uniform cylinder with l/a = 20 matches our expression with a numeric factor of 3/4.

Since we're concerned with the electrostatic energy change per unit length of the plasma, this suggests that the only necessary correction to our calculations assuming an infinite cylinder is, roughly, a factor of two increase in heating.

4.4 Assumptions for Estimating the Diffusion Coefficient

We are interested in the case of diffusion resulting from the broken azimuthal symmetry in a combined solenoidal and multipole field of the form

$$\vec{B} = B_0\hat{z} + B_1\left(\frac{r}{R}\right)^{\alpha-1}(\cos(\alpha\theta)\hat{\theta} + \sin(\alpha\theta)\hat{r}), \tag{4.12}$$

where R is the radius of the multipole, B_1 is the magnetic field of the multipole at this radius, and α is still the above-mentioned order of the multipole.

It has been previously demonstrated that such fields can enhance diffusion of a non-neutral plasma [22]. The following derivation is based, primarily, on work done in [22]. While the process of the derivation is not identical, these heuristic results for the diffusion coefficients differ only by a multiplicative factor of approximately 1.5. Both calculations include only specific low-order drifts and exclude turbulent transport.

4.4.1 Thermal Motion and ExB Drifts

In the limit of a strongly magnetized plasma, large-scale particle motion will consist of primarily two components: a thermal velocity, v_t, along the magnetic field lines and an ExB drift perpendicular to the magnetic field.

$$\vec{v_d} = \frac{\vec{E}\times\vec{B}}{B^2}. \tag{4.13}$$

The component of the thermal velocity along a given coordinate should be proportional to the strength of the magnetic field along that same coordinate. For example, we would expect that

$$\frac{v_{tr}}{v_{tz}} = \frac{B_1}{B_0}\left(\frac{r}{R}\right)^{\alpha-1}\sin(\alpha\theta). \tag{4.14}$$

If we make the additional assumption that $\vec{E} = E(r)\hat{r}$, then we can write down the velocity of a particle, under the drift equation approximation:

$$\begin{aligned} v_z &= \frac{\pm v_t}{\sqrt{1+(\frac{B_1}{B_0})^2(\frac{r}{R})^{2\alpha-2}}} + \frac{B_1 E(r)(\frac{r}{R})^{\alpha-1}\cos(\alpha\theta)}{B_0^2 + B_1^2(\frac{r}{R})^{2\alpha-2}} \\ v_\theta &= \frac{\pm v_t \frac{B_1}{B_0}(\frac{r}{R})^{\alpha-1}\cos(\alpha\theta)}{\sqrt{1+(\frac{B_1}{B_0})^2(\frac{r}{R})^{2\alpha-2}}} - \frac{B_0 E(r)}{B_0^2 + B_1^2(\frac{r}{R})^{2\alpha-2}} \\ v_r &= \frac{\pm v_t \frac{B_1}{B_0}(\frac{r}{R})^{\alpha-1}\sin(\alpha\theta)}{\sqrt{1+(\frac{B_1}{B_0})^2(\frac{r}{R})^{2\alpha-2}}}. \end{aligned} \tag{4.15}$$

We can drastically simplify the system if we also assume that the magnetic field of the multipole is small compared to that of the solenoid at radii with significant plasma density and we neglect all but the lowest order terms in $\beta/B_0\,(r/R)^{\alpha-1}$.

$$\begin{aligned} v_z &= \pm v_t \\ v_\theta &= -\frac{E(r)}{B_0} \\ v_r &= \pm v_t \frac{B_1}{B_0}\left(\frac{r}{R}\right)^{\alpha-1}\sin(\alpha\theta). \end{aligned} \tag{4.16}$$

We should stop to consider what effects we've lost with this assumption. The most pervasive is equivalent to assuming that $\left|\vec{B}\right| = B_0$. This results in a fractional error present in every term, to either first or second order. As such, it is unlikely to qualitatively alter behavior.

The second effect is the azimuthally dependent drift in the z-direction. We note that this is equivalent to the ExB drift of the unperturbed plasma multiplied by our small perturbation parameter and an azimuthal dependence. Thus, this drift will always be much smaller than the unperturbed ExB drift, and the former will cause a comparatively rapid variation in θ that was average the latter out to zero.

The final effect is the azimuthally dependent azimuthal velocity. This is merely a thermal velocity along magnetic field lines. While this velocity is necessarily small due to the smallness of the perturbation, it is not necessarily negligible when compared to the unperturbed ExB drift. In the limit of a high-temperature, low-density plasma, the thermal velocity can be larger than the ExB drift by a factor in excess of the inverse of our smallness parameter, making this the dominant source of azimuthal motion.

In the limit where we neglect the ExB drift, particles will simply stream back and forth along field lines. These field lines converge toward angles given by $\frac{\pi}{2\alpha} + \frac{2\pi N}{\alpha}$, for

integer N. If we also look at the radial velocity of the particles, we see that these angles also correspond to maximum outward radial velocity. This will change the equilibrium distribution of the plasma from a rough cylinder to a twisted flute. Unfortunately, in this limit, particles simply stream back and forth along their single field line, resulting in no net transport.

In the opposite limit, the ExB drift is large compared to the this perturbing angular velocity. This, the perturbation will once again be averaged out over angle and have no net effect. As we don't anticipate that this perturbative angular velocity will significantly affect the radial transport in either limit, we neglect it.

4.4.2 Other Drifts

We have, so far, neglected two other potential sources of motion across field lines. These drifts arise due to the spatial inhomogeneity of the perturbed magnetic field.

The magnitude of the multipole field increases with radius. This leads to a grad-B drift.

$$\begin{aligned} v_{\nabla B} &= -\frac{1}{2} v_\perp r_L \frac{\vec{B} \times \nabla |B|}{B^2} \\ &= -\frac{1}{2} v_\perp r_L \frac{1}{B^2} \vec{B} \times \left(\frac{\alpha - 1}{|B|} B_1^2 \left(\frac{r}{R} \right)^{2(\alpha-1)} \frac{\hat{r}}{r} \right), \end{aligned} \tag{4.17}$$

where $v_\perp$ is the velocity of the particle perpendicular to the field lines, r_L is the Larmor radius, and the direction of the drift reverses for positively charged particles. As we're assuming the strongly-magnetized limit, the Larmor radius must be small compared to any other relevant scale-length, and the perpendicular velocity should be dominated by the cyclotron velocity that, if we assume thermal equilibrium, should be equal to $\sqrt{2} v_t$.

We can see that the magnitude of this drift is necessarily going to be small due to the factors of r_L and our perturbation parameter squared. While this drift may become large compared to the ExB drift, thanks to the factor of the thermal velocity, it will always be quite small compared to the already existing thermal motions of the plasma.

There is also a curvature drift associated with the changing direction of the magnetic field.

$$v_R = \frac{m v_{||}^2}{q B^2} \frac{\vec{R}_c \times \vec{B}}{R_c^2}. \tag{4.18}$$

$\vec{R}_c$ is the radius of curvature of the magnetic field and $v_{||}$ is the velocity parallel to the field lines, equivalent to v_t.

In the usual limit of a comparatively weak multipole field, the radius of curvature of the field is given by,

$$\left(\frac{B_1}{B_0} \left(\frac{r}{R} \right)^{\alpha-1} \right)^2 \vec{R}_c \approx \frac{r}{\alpha - 1} \left(\hat{r} - \tan(\alpha\theta) \hat{\theta} \right).$$

This gives us, to lowest order in the relative multipole strength,

$$v_R \approx -\frac{mv_t^2}{qB_0}(\alpha-1)\left(\frac{B_1}{B_0}\left(\frac{r}{R}\right)^{\alpha-1}\right)^2 \frac{\cos^2(\alpha\theta)}{r}\left(\tan(\alpha\theta)\hat{r}+\hat{\theta}\right).$$

As in the case of the gradient drift, we can see that this drift will be small compared to the thermal velocities along field lines by an additional factor of the magnetic perturbation and the ratio of the Larmor radius to the size of the plasma. Thus, we neglect these drifts, as well.

4.5 Estimating the Diffusive Velocity

We are interested in determining the average radial speed of particles at a given location in the plasma. We will eventually have to consider the thermal distribution of the plasma, but we will start by considering only particles with a given thermal velocity.

The radial velocity depends on θ, which varies with time. If we define $\frac{E(r)}{rB_0} = \omega$, we have

$$v_r = \pm v_t \frac{B_1}{B_0}\left(\frac{r}{R}\right)^{\alpha-1}\sin(\alpha\theta_0 - \alpha\omega t). \tag{4.19}$$

In general, given our assumptions so far, ω is a function of r. However, since the radial velocity itself is first order in the magnetic field perturbation, which we have already assumed to be small, we will assume that the change in r, and the resulting change in ω, is small enough to neglect over a single bounce period. One might note that for the case of a uniform cylinder of plasma, ω is, in fact, constant with radius.

Our formula for the radial velocity has no explicit z-dependence. However, the sign of this velocity depends on the direction of travel along a field line, which necessarily reverses itself twice over a bounce time. The velocity also has a periodic dependence on time. Thus, even if a particle has a large radial velocity, it is highly likely that the particle will return to its original radius, resulting in no average radial displacement, unless we consider collisions.

We are interested in the regime where collisions are the primary mechanism by which this diffusion operates. The velocity of a particle before and after a collision are not significantly correlated, aside from the location of the collision. Therefore, collisional particles that would otherwise move periodically can diffuse outward or inward.

Thus, we want to average over the average time between collisions, τ_c. We will start with the highly collisional case where the collision time is short enough compared to a bounce time that we can neglect the reversal of direction during a bounce. If we also absorb temporarily irrelevant constants into a new constant, A, we proceed with our integral:

$$\begin{aligned}
\frac{\partial r}{\partial t} &= Ar^{\alpha-1}\sin\alpha(\theta_0-\omega t)\\
\int_{r_0}^{r_1} r^{1-\alpha}dr &= A\int_0^{\tau_c}\sin\alpha(\theta_0-\omega t)dt\\
\left[\frac{1}{2-\alpha}r^{2-\alpha}\right]_{r_0}^{r_1} &= \frac{A}{\alpha\omega}\left[\cos\alpha(\theta_0-\omega t)\right]_0^{\tau_c}.
\end{aligned}$$

Of course, for the special case of a quadrupole field, $\alpha = 2$, the integral over space results in a logarithm instead. Suffice it to say, carrying out the equivalent steps for that special case eventually reaches the same result.

$$\frac{1}{2-\alpha}(r_1^{2-\alpha} - r_0^{2-\alpha}) = \frac{A}{\alpha\omega}(\cos\alpha(\theta_0 - \omega\tau_c) - \cos\alpha\theta_0). \tag{4.20}$$

In the limit where $\Delta r \equiv r_1 - r_0$ is small we can make the approximation that $r_1^n - r_0^n = n r_0^{n-1}(r_1 - r_0)$. This, along with some basic trigonometric identities yields

$$\Delta r = \frac{A r_0^{\alpha-1}}{\alpha\omega}\left[\sqrt{2 - 2\cos(\alpha\omega\tau_c)}\cos(\alpha\theta_0 + \alpha\gamma)\right],$$

where γ is a complicated function of the quantity $\alpha\omega\tau_c$. Note that this result, and therefore all following work, is once again consistent with the $\alpha = 2$ case.

Now, we are prepared to average over θ_0. Naively doing so immediately yields zero, as the average of Cosine is zero. However, this is because the naive average cancels out particles traveling outward with particles traveling inward, even though both directions of travel contribute positively to diffusion. After all, for every particle traveling along a magnetic field line, there is an equal probability of a particle traveling in the opposite direction along that same field line. What we need is some measure of the average of the absolute value of the displacement. We'll use the root mean square (RMS) displacement. For a pure Sine or Cosine curve, this is simply $1/\sqrt{2}$.

$$\begin{aligned}\left\langle \Delta r^2 \right\rangle_\theta^{1/2} &= \frac{A r_0^{\alpha-1}}{\sqrt{2}\alpha\omega}\sqrt{2 - 2\cos(\alpha\omega\tau_c)} \\ &= \frac{v_t}{\sqrt{2}\alpha\omega}\frac{B_1}{B_0}\left(\frac{r}{R}\right)^{\alpha-1}\sqrt{2 - 2\cos(\alpha\omega\tau_c)}.\end{aligned} \tag{4.21}$$

In the opposite limit, the collision time is long enough compared to the bounce time that we can treat the path between collisions as an integer number of full traversals. In that case, we can write down an expression for the radial displacement over each traversal in the from of Equation 4.23, with τ_c replaced by τ, the bounce time, and θ_0 adjusted to match the previous traversal. Adding all of these up will give us a rough value for the diffusive radial step over a single collision time.

Unfortunately, this limit becomes much more difficult when we want to average over the original θ_0, as we need to reduce the entire expression to a single trigonometric function to be able to easily calculate its RMS value. However, we can make this reduction for cases where $\tau_c = 2^n\tau$, for whole number n. After averaging over θ_0, we are left with

$$\left\langle \Delta r^2 \right\rangle_\theta^{1/2} = \frac{A r_0^{\alpha-1}}{\sqrt{2}\alpha\omega}\sqrt{2 - 2\cos(\alpha\omega\tau)}\sqrt{2 - 2\cos(\alpha\omega\tau)}\prod_{i=1}^{n-1}\sqrt{2 + 2\cos(2^i\alpha\omega\tau)}. \tag{4.22}$$

Of course, this functional form is not terribly enlightening. We can see that the terms inside the square roots are periodic, with a maximum of $2^{n+1} = \frac{2\tau_c}{\tau}$ whenever $\alpha\omega\tau =$

$N\pi$, for odd N, that becomes ever narrower as n increases. Though, if n becomes too large, the radial excursion between collisions may become large, and our derivation is no longer valid.

If we say that $\tau = l/v_t$, where l is the length of the plasma, then our condition for a maximum in the radial transport becomes $\frac{\alpha\omega l}{v_t} = N\pi$. This makes sense when we consider that $\frac{\omega l}{2v_t}$ is the angular rotation made by a particle on a single pass of the plasma and that $\frac{\pi}{2\alpha}$ is the rotation in the multipole field lines along the same pass. Thus, particles that match these two numbers will be on a trajectory that moves always inward or outward (or not at all for specific initial conditions).

4.6 Estimating the Diffusion Coefficient: Collisional case

A diffusion coefficient must be of the form $D = l_{mfp}^2/\tau_c$, where l_{mfp} is the magnitude of the diffusive steps and τ_c is the time between them. (It may, of course, also be equivalently written in terms of the diffusive velocity.)

We must decide how to turn our diffusive step size at a single thermal velocity into a general diffusion coefficient. Ideally, we would square Equation 4.23, divide by the collision time, and integrate over the thermal distribution to determine the true average. This becomes extremely difficult when we consider that the average collision time for a particle certainly depends on its thermal velocity, but is trivial if we neglect this effect.

We get

$$\begin{aligned} D &= \int_0^{\inf} \frac{1}{\alpha^2\omega^2\tau_c}\left(\frac{B_1}{B_0}\left(\frac{r}{R}\right)^{\alpha-1}\right)^2 (1-\cos(\alpha\omega\tau_c))\sqrt{\frac{m}{2\pi k_B T}} v_t^2 e^{\frac{-mv_t^2}{2k_B T}} dv_t \\ &= \frac{k_B T}{2m\alpha^2\omega^2\tau_c}\left(\frac{B_1}{B_0}\left(\frac{r}{R}\right)^{\alpha-1}\right)^2 (1-\cos(\alpha\omega\tau_c))\,. \end{aligned} \tag{4.23}$$

What does this mean? We recall that this expression is for the case where the collision time is much less than the bounce time. Thus, particles will typically travel a very short distance along the length of the plasma and their radial displacement will largely be governed by their azimuthal displacement, $\omega\tau_c$. If we look at our expression, we see that the diffusion coefficient is zero whenever $\alpha\omega\tau_c = N\pi$, for even N. This corresponds to traversing a full period of the azimuthal variation in the magnetic field, which we would expect to result in zero net displacement. Between these minima, at roughly odd N, are local maxima in the diffusion coefficient, which are damped as $1/N$.

Of course, reaching any of these local maxima requires that $1/\omega$ be comparable to or smaller than τ_c. If the plasma is in the "stiff" regime, where ω is less than the bounce frequency, in addition to the highly collisional regime we're currently considering, then $1/\omega$ will always be much larger than τ_c, and the plasma will be far below the first resonance in Equation 4.25. In that case, we can expand around $\alpha\omega\tau_c = 0$ and get

$$D \approx \frac{k_B T \tau_c}{4m}\left(\frac{B_1}{B_0}\left(\frac{r}{R}\right)^{\alpha-1}\right)^2.$$

However, since this regime was not experimentally realizable for us, this presents mainly a theoretical curiosity.

4.7 Estimating the Diffusion Coefficient: Low-collision case

In the case of a plasma with a relatively low collision rate, our expression for the size of the diffusive steps is more complicated. Thus, the task of integrating this expression over the thermal distribution becomes impossible, analytically.

However, we recall that the width of the resonance at $\frac{\alpha\omega l}{v_t} = N\pi$ becomes smaller and smaller as the collision time becomes relatively larger than the bounce time. So we make the simplification of only considering the particles at or near resonance. Doing this, we no longer need to integrate over the thermal distribution. Instead, we merely multiply by the distribution evaluated at the resonance and an appropriate width of the resonance.

But what is the width of the resonance? We consider the trigonometric terms in Equation 4.24, squared for inclusion in the diffusion coefficient. As we are only interested in the value of the function near resonance, we can expand the Cosines around $\alpha\omega\tau = N\pi$. If we further consolidate temporarily unimportant coefficients, we have

$$\begin{aligned}(\Delta r)^2 &\approx A_1 4^n \left[4 - (\alpha\omega\tau - N\pi)^2 \left(1 + \sum_{i=0}^{n-1} 4^i\right)\right] \\ &= A_1 4^n \left[4 - \frac{(\alpha\omega\tau - N\pi)^2}{3}\left(4^n + 2\right)\right].\end{aligned}$$

We have reduced our expression to a parabola of the form $f(x) = a - bx^2$, for positive a and b. Such a function reaches a maximum of $a \equiv A_1 4^{n+1} = 4A_1\left(\frac{\tau_c}{\tau}\right)^2$ at $x = 0$ and has a full-width at half-maximum of $\sqrt{\frac{2a}{b}} \equiv \sqrt{\frac{24}{4^n+2}} \approx \frac{\sqrt{24}}{2^n} = \sqrt{24}\frac{\tau}{\tau_c}$, for large n. We relate this width in $\alpha\omega\tau$ to the width in v_t by $\frac{\Delta(\alpha\omega\tau)}{\alpha\omega\tau} = \frac{\Delta v_t}{v_t}$.

Putting all of this together, we now have

$$\begin{aligned}\Delta v_t &= \frac{\sqrt{24}l}{N\pi\tau_c} \\ f(v_t) &= \sqrt{\frac{m}{2\pi k_B T}} e^{-\frac{m v_t^2}{2k_B T}} \\ D &= \left[\frac{\langle|\Delta r|\rangle^2}{\tau_c} f\left(v_t\right)\Delta v_t\right]_{\alpha\omega\tau = N\pi} \\ &= \frac{4\sqrt{6}}{N^5\pi^5}\alpha^2\omega^2 l^3 \left(\frac{B_1}{B_0}\right)^2 \left(\frac{r}{R}\right)^{2\alpha-2} \sqrt{\frac{m}{2\pi k_B T}} e^{-\frac{m\alpha^2\omega^2 l^2}{2N^2\pi^2 k_B T}}. \qquad (4.24)\end{aligned}$$

Once again, this agrees with the results presented in [22], up to a multiplicative factor of 1.5.

4.8 Using this result

We can finally combine Equations 4.9 and 4.24, along with our numeric integration results, to estimate the heating of the plasma due to multipole-enhanced diffusion:

$$\begin{aligned}\frac{\partial T}{\partial t} &\approx \frac{\lambda q^2}{2\pi k_B \epsilon_0}\frac{D}{r_p^2} \\ &\approx \frac{4\sqrt{6}q^2}{2\pi^6 k_B \epsilon_0}\frac{\lambda}{r_p^2}\frac{\alpha^2\omega^2 l^3}{N^5}\left(\frac{B_1}{B_0}\right)^2\left(\frac{r_p}{R}\right)^{2\alpha-2}\sqrt{\frac{m}{2\pi k_B T}}e^{-\frac{m\alpha^2\omega^2 l^2}{2N^2\pi^2 k_B T}}. \end{aligned} \tag{4.25}$$

If we wish to rephrase this into a slightly more evocative form, we write

$$\frac{\partial T}{\partial t} \approx (0.009)\frac{q^2}{k_B\epsilon_0}\frac{\lambda}{r_p^2}\frac{\alpha\omega l^2}{N^4}\left(\frac{B_1}{B_0}\left(\frac{r_p}{R}\right)^{\alpha-1}\right)^2\sqrt{\frac{m}{2k_B T}\left(\frac{\alpha\omega l}{N\pi}\right)^2}e^{-\frac{m}{2k_B T}\left(\frac{\alpha\omega l}{N\pi}\right)^2}.$$

What can we take from this? We have that the rate of temperature change is proportional to the density of the plasma times something with the units of a diffusion coefficient- exactly what we had in Equation 4.9. We also see that the diffusion coefficient is proportional to our earlier smallness parameter $\frac{B_1}{B_0}(\frac{r_p}{R})^{\alpha-1}$, which represents the strength of the multipole's magnetic perturbation, squared. Finally, we have a function, $f(x) = \sqrt{x}e^{-x}$, of a dimensionless ratio. This ratio characterizes how close the plasma is to the resonance driving the radial diffusion. When $x = \frac{1}{2}$, we are in resonance and $f(x)$ is maximized.

Unfortunately for the succinctness of this formulation, ω cannot be easily measured and depends on the value of other plasma parameters. Thus, if we want a formula we can actually use, we'll need to determine the value of ω. For the case of the Gaussian distribution mentioned earlier, $\omega(r_p) \approx (.1)\frac{\lambda q}{\epsilon_0 r_p^2 B_0}$. We also note that the diffusion is strongly suppressed for large N and neglect all but N=1 for simplicity.

$$\frac{\partial T}{\partial t} \approx \frac{4\sqrt{6}q^4}{200\pi^6 k_B \epsilon_0^3}\frac{\lambda^3}{r_p^6}\alpha^2 l^3\frac{B_1^2}{B_0^4}\left(\frac{r_p}{R}\right)^{2\alpha-2}\sqrt{\frac{m}{2\pi k_B T}}\exp\left[-\frac{m\alpha^2\lambda^2 q^2 l^2}{200\pi^2\epsilon_0^2 r_p^4 B_0^2 k_B T}\right]. \tag{4.26}$$

In Figure 4.1, we plot the expected plasma heating in an octupole against temperature while varying various plasma parameters.

Of course, the importance of this result is in how it interacts with other sources of heating and cooling, particularly cyclotron cooling. Charged particles in a magnetic field will radiate away energy due to their cyclotron acceleration. The rate of change of their temperature is given by

$$\frac{\partial T}{\partial t} = -\frac{2q^4}{9\pi m^3\epsilon_0 c^3}|B|^2 T, \tag{4.27}$$

which, for an electron, results in an exponential decay in temperature with a time constant of $3.87/B^2$ s.

Note that as cyclotron cooling is a single-particle effect, the cooling rate does not depend on any variable parameter but the magnetic field and the temperature.

We would expect a plasma exposed to both of these effects would reach an equilibrium temperature where the diffusion-enhanced heating balances the cyclotron cooling.

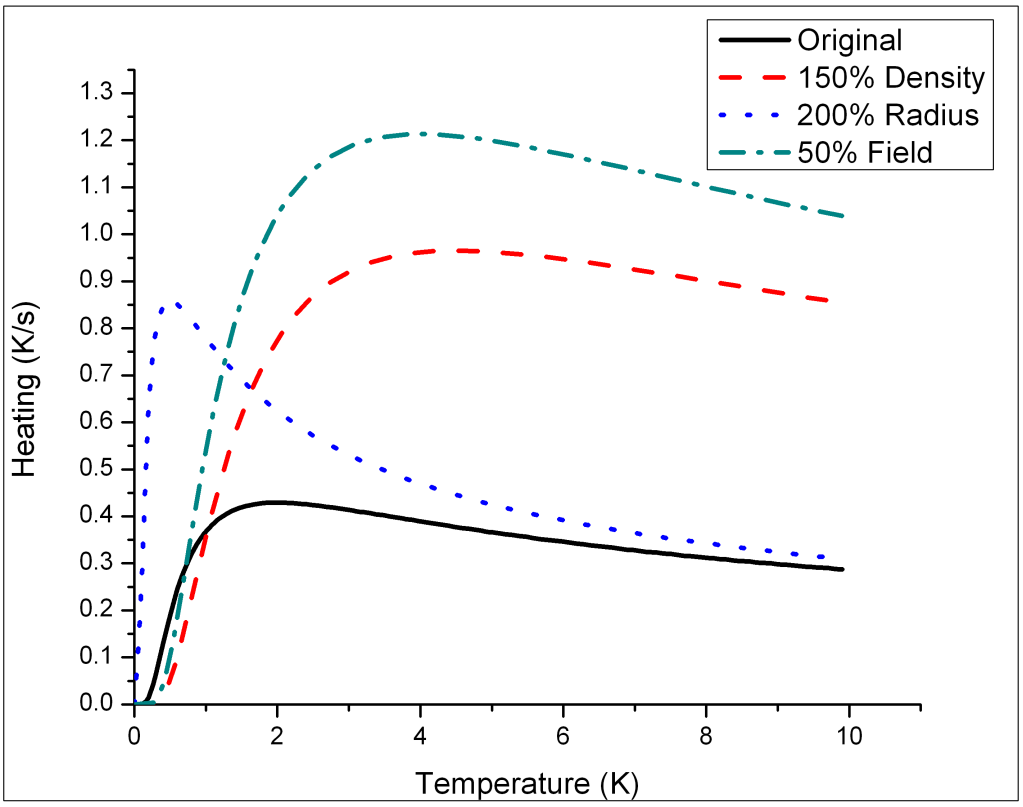

Figure 4.1: Expected plasma heating as a function of temperature: plots of Equation 4.26 as a function of temperature for the case of an octupole field. We see that increasing the plasma density, while keeping the radius constant, or reducing the magnetic field, while keeping the ratio of the multipole and solenoid field constant, increases heating at high temperatures and decreases heating at very low temperatures. Increasing the plasma radius, while keeping all other parameters constant, increases heating at all temperatures, but particularly at low temperatures. Note that we expect alterations in these curves over time in addition to what would be expected from increasing radius and decreasing density, due to diffusion. Note that the values of the plasma parameters used to generate these plots were chosen to emphasize the general trends and are not necessarily representative of experimental plasmas.

To find such equilibria, it is helpful to consider some features of the heating as a function of temperature. Refer again to Figure 4.2. Both the heating and its derivative with respect to temperature go to zero as the temperature approaches either zero or infinity. The heating has a single maximum with respect to temperature and is monotonically increasing below this maximum and monotonically decreasing above this maximum.

There always exists a trivial solution at T=0. Since the derivative of the heating also goes to zero at low temperatures, the cyclotron cooling with always be greater in magnitude than the heating at sufficiently low temperatures. Thus, this equilibrium is also stable.

Since the heating is bounded above while the cooling is not, for sufficiently small values of M and P the heating will always be less than the cyclotron cooling and the only equilibrium will be at T=0.

However, since the heating below resonance increases exponentially with T, for higher values of M and P the heating can overtake the cooling, which only increases linearly with T, resulting in a non-zero equilibrium temperature.

At this equilibrium the heating is increasing more quickly with temperature than the cooling. Thus, the heating will dominate at temperatures above this point and the cooling will dominate at all lower temperatures. Thus, this equilibrium, if it exists, is unstable.

If this equilibrium does exist, it means the heating rate has surpassed the cooling rate. Since the heating rate goes to zero for sufficiently high T, they must also be equal at a third point. However, due to the piece-wise monotonic nature of the heating, this is the last possible equilibrium.

At this point, the heating is either decreasing with temperature or increasing more slowly than the cooling. At even higher temperatures, the cooling will take over, making this equilibrium stable.

There is, of course, the critical case where the second and third equilibria occur at the same temperature. In this case, the cooling is greater than or equal to the heating at all temperatures, resulting in only the single stable equilibrium at T=0.

So, in summary, for plasmas in a parameter regime with sufficiently weak diffusion-enhanced heating, cyclotron cooling will dominate and drive the plasma to 0 K. Other plasmas will be bistable at either 0 K or some single higher temperature.

Determining the condition for bi-stability, the value of the non-zero equilibrium temperature, or the unstable boundary equilibrium is rather difficult, as you are solving an equation of the form

$$T^{3/2} = ae^{-b/T},$$

which cannot be solved analytically.

However, if we're willing to deal with special functions, we can find many solutions, most of which are complex. The solution that interests us, however is

$$T \to \frac{-2b}{3W(\frac{-2b}{3a^{2/3}})},$$

where W(x) is the Lambert W-function, which is defined as the inverse of xe^x.

The relevant features of W(x) to consider are that, for real x, W(x) has no real values for $x < -\frac{1}{e}$, $W(-\frac{1}{e} = -1$, W(x) is double valued for $-\frac{1}{e} < x < 0$, and is single valued for $x > 0$. As we are physically constrained to $x < 0$, we can rephrase the condition on bi-stability as

$$\begin{aligned} \frac{-2b}{3a^{2/3}} &\geq -\frac{1}{e} \\ (\ 0.411)\frac{q^2}{36c^2}\left(\frac{\alpha^2 B_0^2 \pi}{m^4 \epsilon_0^2}\right)^{1/3} &\leq \frac{1}{e}\left(\frac{B_1}{B_0}\left(\frac{r_p}{R}\right)^{\alpha-1}\right)^{4/3}, \end{aligned} \tag{4.28}$$

which, interestingly enough, does not depend on the shape or density of the plasma- merely on the constituent particles, the solenoidal field, and the magnitude of the multipole field perturbation.

For the case of an electron plasma, this reduces to

$$(3.06 \times 10^{-12})\alpha B_0 \leq \left(\frac{B_1}{B_0}\left(\frac{r_p}{R}\right)^{\alpha-1}\right)^2, \tag{4.29}$$

and the question is reduced to simply determining how small our small magnetic perturbation is. For a plasma in our octupole with a 1mm radius, the magnetic perturbation is above this limit by, roughly, a factor of 1000. Thus, we expect most of our plasmas to be well into the bi-stable regime.

The equilibrium temperature just at the point of bi-stability becomes

$$T_{eq} = \frac{m\alpha^2\lambda^2 q^2 l^2}{300\pi^2\epsilon_0^2 r_p^4 B_0^2 k_B} = (7.30 \times 10^{-27})\left(\frac{\alpha\lambda l}{B_0 r_p^2}\right)^2, \tag{4.30}$$

for an electron plasma. If we plug in typical alpha parameters of 10^{15} particles per cubic meter and a length of a few millimeters, we get a temperature of roughly 1K. However, since we expect our plasmas to be far from this critical point, this only serves as a limit separating the high and low equilibrium temperatures.

Once we are well into the bistable regime, the branch of W(x) that continues to positive x passes through W(0) = 0 with a slope of 1, corresponding to the stable equilibrium temperature, which diverges as we pass further and further into this regime. The other branch diverges roughly logarithmically towards $-\inf$, corresponding to the unstable equilibrium, which goes towards 0 as -1/log(x), for $x \to 0$. Note that plasmas below this temperature will stay below this temperature, while those above it will go to the non-zero stable equilibrium.

If we are well into the bistable regime, the argument of the Lambert-W function is small and we can Taylor expand the branch corresponding to the stable equilibrium. This turn out to be equivalent to neglecting the exponential in Equation 4.26, or expanding it around $T \to \infty$. This yields

$$\begin{aligned} (k_B T_{eq})^{3/2} &\approx \frac{24\sqrt{6}m^3c^3}{\pi^3\epsilon_0^2}(.00038)\frac{\lambda^3}{r_p^6}\alpha^2 l^3 \frac{\beta^2}{B_0^6}\left(\frac{r_p}{R}\right)^{2\alpha-2}\sqrt{\frac{m}{2\pi}} \\ T_{eq}^{3/2} &\approx (1.39 \times 10^{-27})\frac{\lambda^3}{r_p^6}\alpha^2 l^3 \frac{\beta^2}{B_0^6}\left(\frac{r_p}{R}\right)^{2\alpha-2}. \end{aligned} \tag{4.31}$$

Plugging in a variety of typical plasma parameters for the ALPHA experiment yields temperatures ranging from 10-1000K.

Unfortunately, the branch of W(x) corresponding to the unstable equilibrium cannot be expanded in this way.

4.9 Additional Examples

It may be helpful to consider and compare to the heating caused by other sources of diffusion.

One of the strongest sources of diffusion for a plasma is Bohm diffusion, also known as anomalous diffusion. In this case, turbulence in the plasma gives rise to ExB drifts causing orbits much larger than the cyclotron orbit, enhancing classical diffusion across a magnetic field.

$$D_B = \frac{1}{16}\frac{k_B T}{qB}.$$

Of course, this is generally observed in neutral plasmas, which we are not dealing with. However, the name Bohm diffusion is applied to any diffusion process with the same scaling.

Regardless, if we combine this expression with Equation 4.7, we get

$$\frac{\delta T}{\delta t} = \frac{q}{48\pi\epsilon_0}\frac{\lambda}{r_p^2}\frac{T}{B}.$$

If we combine this with the equivalent formula for cyclotron cooling, while simply plugging in the value of various constants for a pure electron plasma, we get

$$\frac{\delta T}{\delta t} \cong 10^{-10}\frac{\lambda}{r_p^2}\frac{T}{B} - \frac{1}{4}B^2 T.$$

This easily solved differential equation permits only exponential growth or decay of the temperature. The only stable equilibria are at T = 0 or $+\infty$. There is also a finite unstable equilibrium, but it requires fine-tuning of the plasma parameters relative to the magnetic field and would be almost always irrelevant.

However, the plasma radius is necessarily an ever-increasing function of time, as the heating is driven by diffusion. This will cause any plasma that happened to be at the unstable equilibrium to immediately begin cooling, and eventually halt the exponential growth of a plasma with a temperature above that point, conveniently removing the solution at $+\infty$ from the achievable and leaving T = 0 as the only solution.

Numerical solution of the differential equation, as well as dimensional analysis, tell us that the time required for a plasma initially being heated by Bohm diffusion to begin cooling is $\tau \approx r_p^2/D_B$, which is on the order of milliseconds for plasmas of interest to us.

Chapter 5

Observations

5.1 Overview

The theoretical models in the previous chapter make, essentially, two different predictions. First, the introduction of a multipole field may enhance diffusion of a plasma. Second, this diffusion may increase the temperature of the plasma.

Thus, we will first attempt to predict the behavior of our experimental plasmas under these two effects, separately, and compare this behavior to experimental observations before attempting to do the same with the total effect.

5.2 Diffusion

5.2.1 Short Times

As established in the previous chapter, we expect a plasma undergoing uniform diffusion to increase in RMS radius a, if it is sufficiently small compared to the size of the electrodes, according to

$$D = \frac{a}{2}\frac{\partial a}{\partial t}.$$

Unfortunately, our model predicts a spatially varying diffusion coefficient, in which case we cannot analytically solve the diffusion equation. However, if the plasma is particularly small the spatial variation in the diffusion coefficient across the plasma may be negligible. In this case, we can replace the diffusion coefficient with its average over the plasma distribution, which may vary in time as the plasma expands.

The simplest reasonable case is to assume the diffusion has a monomial dependence on the plasma size, $D = D_0 a^p$. We note that this is roughly the relation predicted by our model, in the high-temperature limit. We can solve the resulting differential equation by integration.

$$D_0 a^p = \frac{a}{2}\frac{\partial a}{\partial t}$$

$$\begin{aligned} 2D_0 dt &= a^{1-p} da \\ 2(2-p)D_0 t &= a^{2-p} - a(0)^{2-p} \\ a(t) &= \left(a(0)^{2-p} + 2(2-p)D_0 t\right)^{\frac{1}{2-p}} . \end{aligned}$$

Or, if p=2, the solution becomes $a(t) = a(0)e^{2D_0 t}$.

We can sort all possible cases into two easily distinguished qualitative groups, separated by the p=1 case. If the diffusion coefficient scales with the plasma radius more rapidly than linearly, the rate of plasma expansion will increase over time. If the diffusion coefficient scales more slowly, or even inversely with size, the plasma expansion will decrease over time.

However, for values of p greater than 2, this simplified model predicts a divergence to infinite radius over a finite time. This is, clearly, a non-physical result. Of course, this is not unexpected, as the assumption that the diffusion coefficient is roughly constant over the entire plasma is clearly invalidated long before the plasma reaches an infinite radius.

To see what this means for our model of the diffusion coefficient, we consider our earlier formula for it, in the high temperature limit and simplified for the case of an electron or positron plasma:

$$D \approx \left(1.1 \times 10^{-23}\right) \frac{\lambda^2 l^3}{r_p^4} \left(\frac{r}{R}\right)^{2\alpha-2} \frac{\alpha^2}{B_0^2 \sqrt{T}} \left(\frac{B_1}{B_0}\right)^2 . \tag{5.1}$$

Replacing the radial coordinate with the plasma radius (the average of the former over the distribution will certainly be at least proportional to the latter) and inserting it into the previous result predicts that the growth rate of the plasma ($\frac{\partial r_p}{\partial t}$) would increase over time for octupole and higher order multipoles, and decrease over time for lower order multipoles, with the actual threshold being at $\alpha = 3.5$, the physically unachievable septupole.

This model also assumes that D_0 is not a function of time. However, the diffusion coefficient depends on the temperature of the plasma, in addition to its spatial distribution. If the diffusive heating of the plasma is strong enough, the temperature will increase and D_0 becomes a function of time. Thus, this model only holds in the limit where diffusive heating is not a significant determining factor of the plasma temperature.

We can consider the opposite limit, where the plasma temperature is entirely determined by the balance of diffusive heating and cyclotron cooling, if we consider our earlier formula for the equilibrium temperature of the plasma, once again in the high temperature limit and simplified for the case of an electron or positron plasma:

$$T_{eq}^{3/2} \approx \left(1.13 \times 10^{-27}\right) \left(\frac{\lambda l}{r_p^2}\right)^3 \frac{\alpha^2 B_1^2}{B_0^6} \left(\frac{r_p}{R}\right)^{2\alpha-2} .$$

If we plug this into the previous expression for the diffusion coefficient, we get

$$D \approx \left(1.1 \times 10^{-14}\right) \frac{\lambda l^2}{r_p^2 B_0^2} \left(\alpha B_1\right)^{4/3} \left[\left(\frac{r}{R}\right)^2 \left(\frac{r_p}{R}\right)^{-2/3}\right]^{\alpha-1} . \tag{5.2}$$

This results in the same solution as the previous model, though the transition from an expansion rate that decreases over time to one that increases now occurs at $\alpha = 3.25$. So, the qualitative result is the same for all constructable multipoles, including the divergence for multipoles of order higher than 4.

Of course, in the physical case, the diffusive heating of the plasma will be only one of several contributors to the plasma temperature. Unfortunately, there are no simple analytic solutions to cases intermediate to the two we've just considered. Regardless, we expect the true solution to lie between the two, qualitatively very similar, approximate solutions.

5.2.2 Intermediate Times

There are two additional effects that must be considered to extend this model to intermediate times.

First, on time scales of roughly $r_p^2/2D$ the plasma changes shape. This reduces the diffusive heating of the plasma. However, as this effect will merely move the plasma closer to one of the short time solutions we've already considered, it doesn't warrant additions to the model.

Secondly, the assumption that the diffusion coefficient is uniform over the entire plasma becomes worse and worse as time goes by, even resulting in blatantly unphysical solutions for some cases. To avoid this, we must solve the diffusion equation for the case of a spatially varying diffusion coefficient. Unfortunately, this can only be done, in general, numerically.

These numerical results can vary tremendously based on the initial conditions of the plasma and the details of the perturbing magnetic field. However, we see two limiting behaviors that seem to be universal. First, at short times, the numerical solution agrees with the results obtained by ignoring the change in the diffusion coefficient across the plasma. Second, at later times, the plasma expands more and more slowly, appearing to grow as between the square root of time and its logarithm. The transition between these two states generally occurs on a time scale consistent with that expected for a spatial reorganization of the plasma.

In Figure 5.1 we present the numerical solutions of the diffusion equation for the expansion of a plasma over time in a multipole field, with the diffusion coefficient derived above, for a variety of situations of interest.

5.2.3 Late Times

At late times, we must consider that there is an upper limit to the size the plasma will reach via diffusion, set by the size of the confining electrodes. Once particles can reach the electrodes, they will be lost from the plasma and the total number of particles will decrease over time, while the spatial distribution comes into equilibrium.

Unfortunately, the process is not even as simple as this. A plasma is not a truly continuous medium. It consists of discrete particles undergoing complex motions between collisions. As described earlier, these particle orbits may often have quite considerable radial excursions. Thus, even before the smooth density distribution of the plasma hits

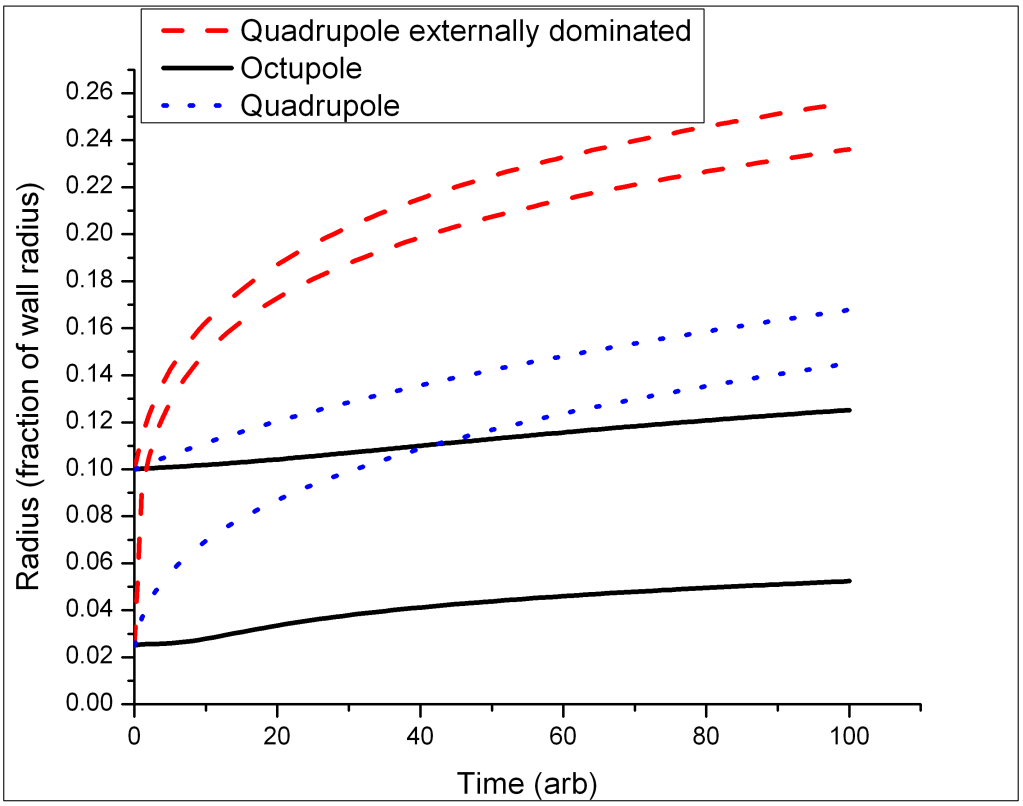

Figure 5.1: Numerical solutions to the non-uniform diffusion equation: In these curves we vary the size of the plasma while holding the total number of particles constant, the order of the multipole magnet, and the importance of external heating. For the curves labeled Quadrupole externally dominated, it is assumed that the temperature of the plasma is set entirely by external sources of heating. For the curves labeled Quadrupole, it is assumed that the temperature of the plasma is driven primarily by the expansion of the plasma. Thus, the temperature of the plasma rises as it expands and the diffusion is suppressed. This distinction is not made for the Octupole, as the numerical scaling is unaffected. In all cases, it is assumed that the starting temperature is significantly above resonance.

it, individual particle will be able to follow ballistic trajectories onto the wall. This effect, potentially, places an even lower upper limit on the size of the plasma.

To evaluate the potential impact of this effect, we first recall the form of the magnetic field in the trap:

$$\vec{B} = B_0\hat{z} + B_1\left(\frac{r}{R}\right)^{\alpha-1}(\cos(\alpha\theta)\hat{\theta} + \sin(\alpha\theta)\hat{r}).$$

Particles can be lost ballistically to the wall when they are on a field line that intersects the wall. Those that do so first are those with the maximum radial excursion, which are those at $\sin(\alpha\theta) = 1$. If we assume that such a field line passes through an arbitrary point (r=r_0, z=0), we can find the radial location of that field line, r(z), at any z using

$$\frac{dr(z)}{dz} = \frac{B_r}{B_z} = \frac{B_1}{B_0}\left(\frac{r(z)}{R}\right)^{\alpha-1}.$$

Solving this equation, for the case of an octupole ($\alpha = 4$) yields

$$r(z) = r_0/\sqrt{1 - 2z\frac{B_1}{B_0}\frac{r_0^2}{R^3}}.$$

If a plasma held in a trap is subjected to the introduction of a multipole field, we expect the ends of the plasma to deform symmetrically, while the center of the plasma remains relatively unchanged [23]. Thus, the relevant maximum value for z is half the length of the plasma, l_p.

So, if r($l_p/2$) $\geq$ R for any r_0 where the plasma has a significant density, particles will be subject to this ballistic loss. The critical radius, when this begins to occur, is given by

$$r_c = R/\sqrt{1 + \frac{l_p}{R}\frac{B_1}{B_0}}.$$

While this treatment only considered those field lines with maximum radial excursion, the plasma will rotate azimuthaly over time, eventually bringing any particle onto such a line. As a result, both simulations and experiments [16] show that particle loss occurs quite quickly for plasmas that meet this criteria.

However, by design, most of the plasmas considered here are small enough, both longitudinally and azimuthally, that this effect is not a significant concern.

5.2.4 Observations

Unfortunately, observations of real plasmas in real magnetic fields have the added complication that the magnets producing the multipole field cannot be turned on instantaneously. Our octupole can be, typically, ramped up to its full current over no less than

30s. This time scale is comparable to the expected diffusive time scales, making comparison with the simple analytical models problematic. Fortunately, the numerical model are entirely capable of considering time-varying parameters.

Additionally, the experimental situation in the real world is not nearly as plastic as theoretical space. Thus, we cannot compare experimental results to the model of expansion presented here in its full generality, but only in the specific situation of our experimental apparatus.

In Figure 5.2, we present the expansion of a plasma over time as the octupole magnet is turned on and left at full current along with the results of our model for the same case.

5.3 Heating

We also have a quite extensive model for the heating of a plasma undergoing diffusion in a multipole field. However, the principles behind it are applicable regardless of the reason for the plasma's expansion. This is, if we know the size of the plasma as a function of time, we can directly solve eq 4.6 without any reference to diffusion.

In Figure 5.3, we present the temperature of the plasma undergoing the expansion depicted in Figure 5.2. We also show a value for the expected temperature of the plasma, assuming that its temperature is set entirely by the balance between expansion-driven heating and cyclotron cooling. This value is calculated based solely on the observed expansion of the plasma.

However, it is often the case that we care about the heating of a plasma more than any expansion that plasma might be undergoing. Thus, we would like to have a description of the heating of the plasma that doesn't require us to first either measure or solve for the plasma's expansion.

Leading up to Equation 4.9, we found that, for the drastically simplified case of free, uniform diffusion,

$$\frac{\partial T}{\partial t} \approx \frac{\lambda q^2}{6\pi k_B \epsilon_0} \frac{1}{r_p} \frac{\partial r_p}{\partial t}.$$

If we consider the case of an octupole magnet, we also found that, for short times, the plasma radius expands as $r_p \approx r_{p0} e^{2D_0 t}$. Plugging this in to the previous equation yields

$$\frac{\partial T}{\partial t} \approx \frac{\lambda q^2}{3\pi k_B \epsilon_0} D_0.$$

However, we also found that, at later times, the plasma's expansion slows. For the sake of simplicity, assume that the plasma makes an immediate transition to expanding as $b + c/ln(t)$ at some time t_1, where b and c are constants chosen to maintain continuity of the plasma radius and its first derivative. Plugging this into our approximation for the plasma heating yields

$$\frac{\partial T}{\partial t} \approx \frac{\lambda q^2}{3\pi k_B \epsilon_0} D_0 \frac{t_1}{t} \frac{r_p(t_1)}{r_p}.$$

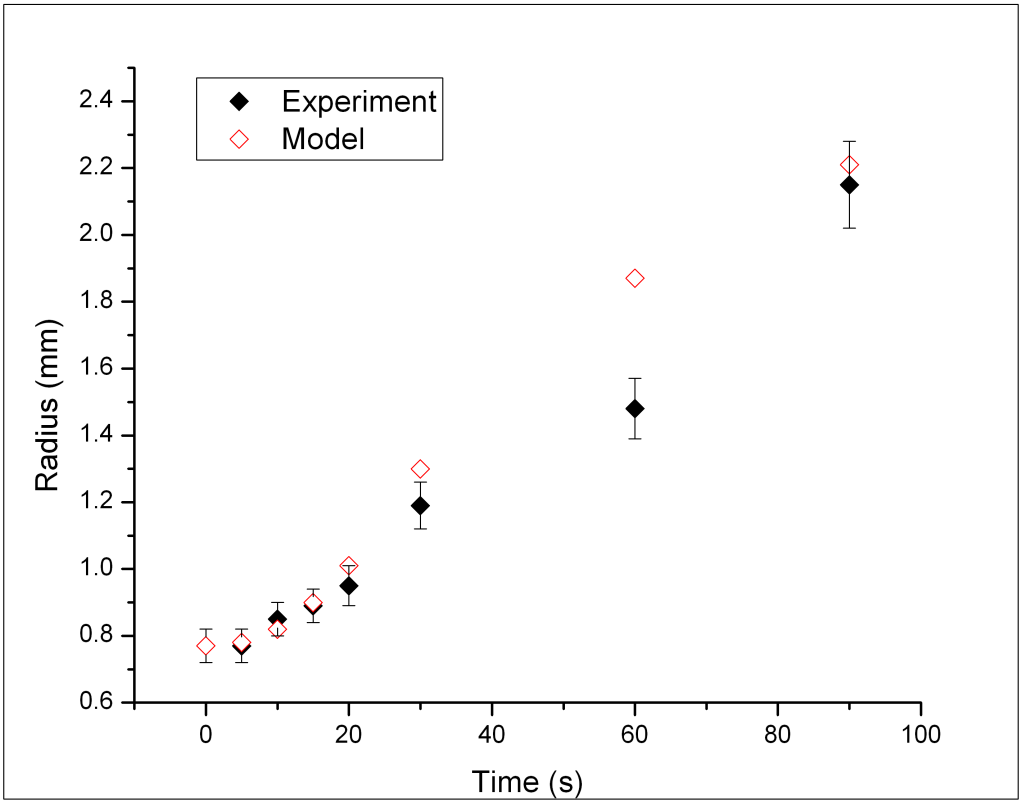

Figure 5.2: Expansion of a plasma in the octupole: we begin the ramping of the octupole magnet at t=0 and it finishes at t=30s. The model comes from a numerical solution of the diffusion equation with the diffusion coefficient given by Equation 5.2 and an initial density of 10^{15} particles per cubic meter. Recall that, as our measurement of the plasma radius is destructive, data points represent individually prepared and evolved plasmas. Error bars represent systematic errors

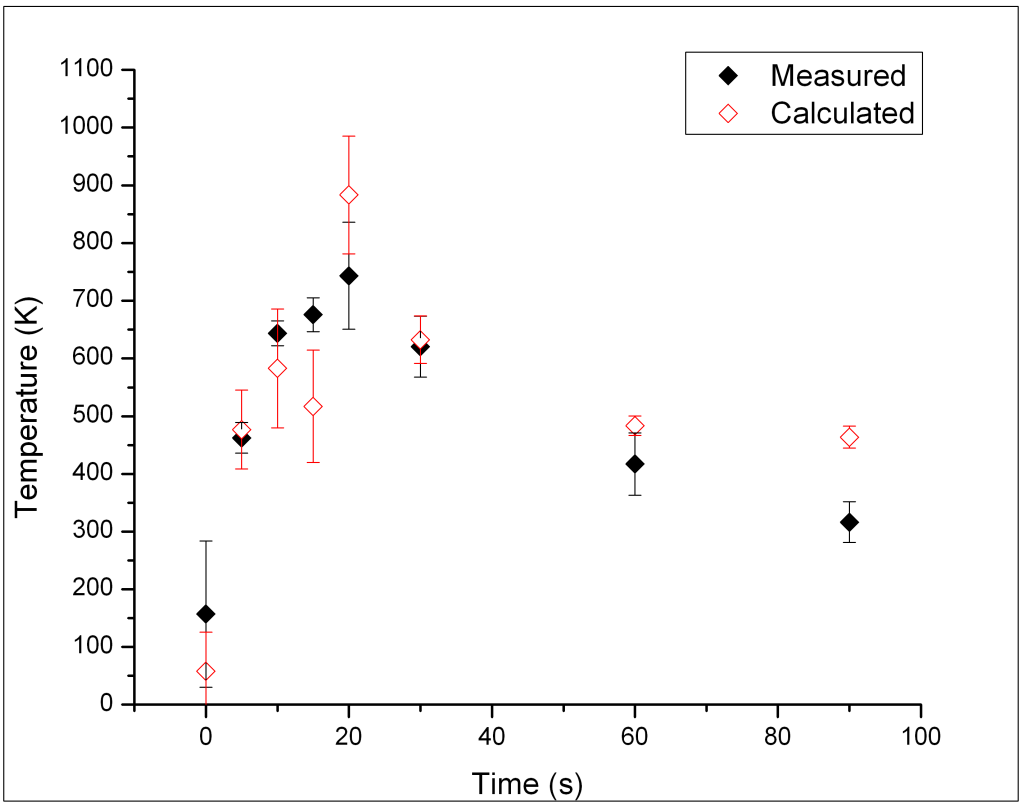

Figure 5.3: Heating of an expanding plasma: the measured (black) points represent the temperature resulting from the same plasma parameters and multipole field behavior as in Figure 5.2. The calculated (red) temperatures are based solely on the expansion observed in Figure 5.2. As this calculation is based on experimental data, it is given error bars based on the propagation of errors in that data.

We can test this approach by directly integrating the numerical solutions of the diffusion equation described in the previous section. Unfortunately, for the case of spatially varying diffusion, this approach turns out to produce results that are merely evocative of the numerical results. That is, it correctly predicts that the heating will decrease and over roughly the correct time-scale, but does not match the functional form of the numerical results.

We might also expect the heating to decrease similarly to $\left(1 - S\left(\frac{r_p(0)}{2D(0)t}\right)\right)$, a function defined in Equation 4.10 and derived for the case of uniform bounded diffusion.

This slightly more complex analytic approach, thankfully, matches quite will with numerical results for those particular varieties of non-uniform diffusion coefficients of interest to us.

5.4 Effects of Finite Temperatures

Unfortunately, all of our previous attempts to determine the expected temperature of the plasma neglected all potential sources of plasma heating or cooling, outside of expansion-driven heating and cyclotron cooling. This was done out of necessity as, even for the simplest possible case of a uniform heating applied to individual particles, the equations become, analytically, completely intractable.

To consider these cases, we need to take a step back, and consider only the heating caused by the diffusive expansion, simplified here to the case of a lepton plasma in an octupole.

$$\frac{\partial T}{\partial t} \approx (5.76 \times 10^{-27}) \left(\frac{\lambda l_p}{r_p^2}\right)^3 \frac{B_1^2}{B_0^4} \left\langle \left(\frac{r}{R}\right)^6 \right\rangle \frac{1}{\sqrt{T}} e^{-(1.75\times10^{-25})\frac{\lambda^2 l_p^2}{r_p^4 B_0^2 T}},$$

where we've temporarily ignored the reduction in heating over time caused by the spatial reorganization of the plasma.

For purposes of comparison with experiment, we may wish to rephrase our expression in terms of the central density of the plasma, n_0, instead of the linear charge density, λ. In that case, we have

$$\frac{\partial T}{\partial t} \approx (1.07 \times 10^{-24}) (n_0 l_p)^3 \frac{B_1^2}{B_0^4} \left(\frac{r_p}{R}\right)^6 \frac{1}{\sqrt{T}} e^{-(1.73\times10^{-24})\frac{n_0^2 l_p^2}{B_0^2 T}}. \tag{5.3}$$

This heating has a maximum, with respect to temperature at

$$\begin{aligned} T_M &\approx (3.46 \times 10^{-24}) \left(\frac{n_0 l_p}{B_0}\right)^2 \\ \frac{\partial T}{\partial t}(T_M) &\approx (3.6 \times 10^{-13}) (n_0 l_p)^2 \frac{B_1^2}{B_0^3} \left(\frac{r_p}{R}\right)^6. \end{aligned}$$

For lepton plasmas used in ALPHA, the temperature of maximum heating is typically between 1 and 1000K. Unfortunately, almost all of our plasmas fall in this temperature range. For the same plasma parameters, the rate of heating is on the order of 1000K/s or higher. Thus, any plasma near this temperature will not remain there for long

We can compare this to cyclotron cooling at the same temperature, as done in chapter 4 with greater generality.

$$\frac{\partial T}{\partial t}(T_M) \approx -(8.65 \times 10^{-25}) \left(n_0 l_p\right)^2 .$$

As in chapter 4, we see that this comparison comes down entirely to the size of the magnetic perturbation and the background magnetic field. For typical ALPHA plasmas, this perturbation is always large enough that the maximum diffusion-driven heating will be stronger than cyclotron cooling at the same temperature, though usually only be a factor of 10.

If the maximum heating due to diffusion were much less than cyclotron cooling at this temperature, it would be much less at all other temperatures, as well. Thus, the diffusion based heating should have minimal effect on the temperature, even when other sources of heating are considered.

If the heating were much greater than the cyclotron cooling at T_M, then we enter the strongly bifurcated regime where cyclotron cooling, and thereby equilibrium, can win out only at temperatures much greater than or less than T_M.

Unfortunately, without prior assumptions or lengthy series of measurements, we do not necessarily know how any additional sources of heating behave with the various plasma parameters or if they are, potentially, affected by the same magnets that result in the enhanced diffusion. However, one thing is almost certain. Without the contribution of the enhanced diffusion, the plasma will reach some equilibrium temperature, T_0, under the influence of cyclotron cooling and these additional heating sources. Comparing T_0 and T_M allows us to anticipate how the plasma temperature will behave under the influence of both (or all) sources of heating.

If T_0 is much greater, then the temperature will certainly remain much greater when the diffusion-based heating is introduced. This places the plasma in the high temperature limit, where our expression for the heating can be drastically simplified. Additionally, since the multipole-enhanced diffusion is suppressed at high temperatures as $1/\sqrt{T}$, the heating should also be suppressed.

If the two temperatures are comparable, then we would expect the diffusion-based heating to be maximized, at least initially. The impact this has on the temperature of the plasma, however, depends on the relationship between the diffusion-based heating and cyclotron cooling. So long as the former is not negligible in comparison to the latter, we would expect the plasma temperature to increase significantly, and likely settle somewhere in the high-temperature limit. Otherwise, we still would not expect notable heating.

If T_0 is much less than T_M, the plasma will start in the low temperature limit, where diffusion is suppressed even more strongly than in the high temperature limit. Thus, unless the diffusion-based heating is much stronger than cyclotron cooling, the plasma should remain cold. However, determining what would happen in the other case requires a slightly more complicated analysis.

In such a case, we can also compare the diffusion based heating and cyclotron cooling at T_0, instead of T_M. If the heating is much greater, the plasma may heat up, though it will likely not heat up into the high-temperature limit, making any attempted calculation of the temperature particularly cumbersome. If the heating is much less, the

Density ($10^8 cm^{-3}$)	Radius (mm)	Initial Temp (K)	Final Temp (K)
4.49	0.52	44	44
4.01	0.51	55	64
15.1	0.28	57	247
8.13	0.37	56	135
11.0	0.46	59	359
4.27	0.77	61	94
2.65	0.44	44	46
7.53	0.28	44	102
3.98	0.28	36	42
4.65	0.26	40	41
0.41	0.83	29	35
18.1	0.36	65	454
2.13	0.69	36	57
2.48	0.64	43	49
6.98	0.57	56	175
17.4	0.22	50	177
15.7	0.21	41	65
11.8	0.92	51	383
9.32	0.36	49	127
2.69	0.66	51	51

Table 5.1: The data presented in Figure 5.4

plasma should not heat significantly. If these two values are comparable, we remain in a regime where the temperature behavior of the plasma may be rather chaotic.

5.5 Observations of Finite Temperature Plasmas

In Table 5.1, we present the temperature of a wide variety of plasmas after heating in the octupole, and without heating in the octupole. The temperatures are measured immediately after the octupole has reached full field, or after an equivalent waiting time.

For almost all of these plasmas, T_M is comparable to T_0 and the expected heating of the plasma is either comparable to or much greater than the expected cyclotron cooling. Thus, we're in a regime where significant heating of the plasma is entirely possible, though not certain.

In order to more accurately predict whether the plasma will heat in the octupole, or to what temperature it will heat to, we need to make some assumptions regarding the behavior of whatever source of heating results in the initial temperature of the plasma. The simplest possible assumption, of course, is that this heating doesn't depend on the plasma temperature or any of the other plasma parameters. In that case, we can simply balance this unchanging source of heating, P_B, against cyclotron cooling.

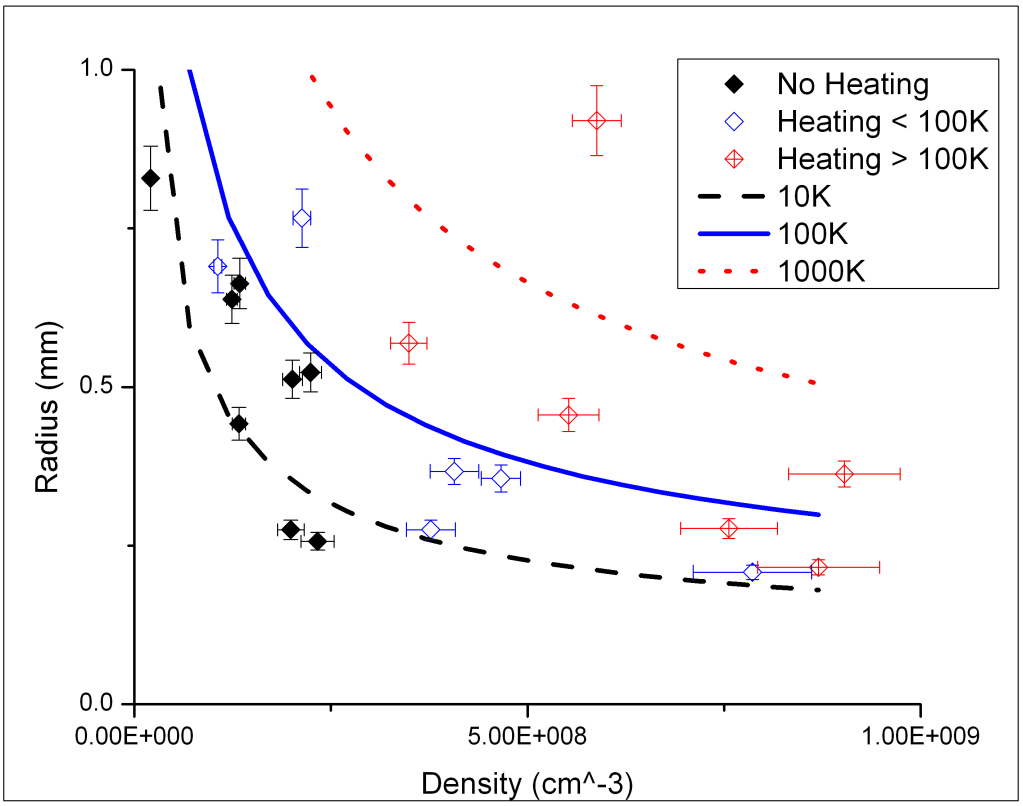

Figure 5.4: Heating of finite temperature plasmas in the octupole: points represent sets of plasma parameters where temperature measurements were performed both after the introduction of the octupole field and without the field, but with an equivalent wait time. Points are classified by the temperature difference between these two cases. Uncertainty in the temperature measurements is, at the very best, on the order of 5K, so differences of 10K or less are compatible with no heating. Lines represent theoretical predictions of sets of plasma parameters where the stated temperature difference is expected to occur. Ideally, all points of a given color would be below the line of the same color and above any lower-temperature lines.

$$P_B - (0.258)\left|B_0^2\right| T_0 = 0.$$

We can then add the diffusion-based heating, P_D, we've been considering.

$$(0.258)\left|B_0^2\right| T_0 - (0.258)\left|B_t^2\right| T + P_D = 0$$
$$T - T_0 = \frac{P_D}{(0.258)B^2}.$$

We assume that the octupole field is effectively a perturbation on the plasma and make the approximation that the magnitude of the magnetic field doesn't change. We will also assume that the change in plasma parameters during the ramping of the octupole magnet is small. We could, in principle, numerically determine an expected change for each of the plasmas under consideration. However, the final result is not sensitive enough to the plasma radius to necessitate the correction.

Figure 5.4 presents the results of this approximation as contours of constant expected heating, along with the plasmas from Table 5.1 classified by the magnitude of observed heating. Considering the number of approximations used in calculating the contours. The agreement with observation is relatively remarkable.

5.6 Other Particle Species

One might recall that we deal in particles other than electrons and positrons: antiprotons. These particles are also held in the octupole field prior to antihydrogen formation and may also heat. Thankfully, it is simple to re-generalize the results of the preceding sections.

The temperature where diffusive heating is maximized increases with the mass of the particles in question, assuming they possess only a single elementary charge.

$$T_M \approx (3.46 \times 10^{-24})\frac{m}{m_e}\left(\frac{n_0 l_p}{B_0}\right)^2.$$

The expected diffusion-driven heating at that temperature is, in fact, not changed. However, the rise in temperature due to that heating increases greatly as cyclotron cooling scales as the inverse of the particle mass cubed. This has the unfortunate effect of driving the cyclotron equilibration time out to several centuries, making it impossible to realistically measure the equilibrium temperature.

Thus, if we took one of the electron plasma considered in the previous section and replaced the electrons with antiprotons, the temperature increase at T_M would increase by a factor of roughly 10^{10}. However, the value of T_M would rise by a factor of roughly 2000. Thus, if the plasma was originally near T_M for an electron plasma, it will be far into the low-temperature limit as an antiproton plasma, reducing any heating predicted by this model to essentially nothing. So, we would not expect such a plasma to heat observably.

Of course, the other plasma parameters, such as density and size, can also vary. Reducing the density of the plasma may bring T_M back down without compromising the heating too strongly. However, this has a limit once the antiprotons become sparse enough to stop acting as a plasma and the assumptions underlying our model for diffusion fall apart. Regardless, heating was never observed in an experimentally relevant antiproton cloud.

5.7 Conclusions

We see that plasmas in the field of our octupole magnet undergo increased radial expansion and Joule heating consistent with our model of multipole-enhanced diffusion. Specifically, by carefully selecting the plasma parameters we can render these effects negligible.

If we wish to minimize the heating of the plasma for a given value of the diffusion coefficient, we must minimize the plasma density, as that is the only other variable parameter that the heating depends on. Unfortunately, reducing the density of our plasmas would also reduce the formation rate of antihydrogen. Thus, this may not be an ideal route for optimization.

There are two possible avenues for minimizing the diffusion of the plasma. The first is to minimize the magnetic perturbation that drives the diffusion: $\left(\left(\frac{r_p}{R}\right)^{\alpha-1}\frac{\beta}{B_0}\right)^2$. Of course, since reducing β/B_0 reduces our capacity to actually trap antihydrogen, this essentially boils down to keeping the plasma as small as possible.

The second avenue is to avoid the resonance that drives the radial diffusion. The principle resonance occurs when $(\alpha\omega l_p/\pi)^2 = k_B T/m$. Recall that the frequency of the plasma's ExB rotation, ω, is linearly proportional to the ratio of the plasma density to the magnetic field. We can avoid this resonance by making the right hand side of the equality larger than the left side. This is the regime most of our lepton plasmas appear to be in. Unfortunately, our model predicts that the heating of the plasma will decrease rather slowly as we move farther into this regime. Additionally, we can only move the plasma farther into this regime by increasing its temperature, which is contrary to the entire point; reducing the the plasma density, which we've already established is less than ideal; reducing the plasma length, which is generally already at the minimum set by the physical size of the electrodes; or increasing the solenoidal magnetic field, which will reduce the depth of the neutral atom trap.

On the other side of the resonance, however, all of these factors work in our favor, and steps that move us farther from resonance will likely increase our trapping efficacy. The model also predicts that the heating of the plasma will fall off quite quickly on this side of resonance. This appears to be the regime that our antiproton clouds are generally in. Unfortunately, our model neglects any effects this change in plasma parameters would have on the temperature of the plasma before the introduction of the multipole field. Thus, attractive though it may be, it might not be mechanically possible for us to move our lepton plasmas to the low-temperature side of resonance.

Bibliography

[1] G. Luders. Proof of the tcp theorem. *Annals of Physics*, 2(1):1–15, April 1957.

[2] C. L. Cesar et al. Two-photon spectroscopy of trapped atomic hydrogen. *Physical Review Letters*, 77(2):255–258, July 1996.

[3] G. B. Andreson et al. Trapped antihydrogen. *Nature*, 468(7324):673–677, December 2010.

[4] H. Dehmelt. Experiments with an isolated subatomic particle at rest. *Review of Modern Physics*, 62(3):525–530, July 1990.

[5] C.M. Surko and R.G. Greaves. Emerging science and technology of antimatter plasmas and trap-based beams. *Physics of Plasmas*, 11(5):2333–2348, May 2004.

[6] G. Gabrielse et al. First capture of antiprotons in a penning trap: A kiloelectronvolt source. *Physical Review Letters*, 57(20):2504–2507, November 1986.

[7] G. Gabrielse et al. Cooling and slowing of trapped antiprotons below 100 mev. *Physical Review Letters*, 63(13):1360–1363, September 1989.

[8] G. B. Andreson et al. Evaporative cooling of antiprotons to cryogenic temperatures. *Physical Review Letters*, 105(1):13003, December 2010.

[9] G. B. Andreson et al. Compression of antiproton clouds for antihydrogen trapping. *Physical Review Letters*, 100(20):203401, May 2008.

[10] G. B. Andreson et al. Antiproton positron and electron imaging with a microchannel plate/phosphor detector. *Review of Scientific Instruments*, 80(1):123701, December 2009.

[11] M.D. Tinkle, R.G. Greaves, C.M. Surko, R.L. Spencer, and G.W. Mason. Low-order modes as diagnostics of spheroidal non-neutral plasmas. *Physical Review Letters*, 72(3):352–355, January 1994.

[12] G. Bendiscioli and D. Kharzeev. Antinucleon-nucleon and antinucleon-nucleus interaction: a review of experimental data. *La Revista del Nuovo Cimento*, 17(6):1–42, 1994.

[13] G. B. Andreson et al. Particle physics aspects of antihydrogen studies with alpha at cern. *AIP Conference Proceedings*, 1037(208), 2008.

[14] F. Robicheaux. Three-body recombination for electrons in a strong magnetic field: Magnetic moment. *Physical Review A*, 73(3):033401, March 2006.

[15] W. Bertsche et al. A magnetic trap for antihydrogen confinement. *Nuclear Instruments and Methods in Physics Research A*, 566:746–756, July 2006.

[16] J. Fajans N. Madsen and F. Robicheaux. Critical loss radius in a penning trap subject to multipole fields. *Physics of Plasmas*, 15(3):032108, March 2008.

[17] B.R. Beck. *Measurement of the Magnetic and Temperature Dependence of the Electron-Electron Anisotropic Temperature Relaxation Rate*. PhD thesis, University of California - San Diego, 1990.

[18] G. B. Andreson et al. Centrifugal separation and equilibration dynamics in an electron-antiproton plasma. *Physical Review Letters*, 106(14):145001, April 2011.

[19] T.M. O'Neil. Centrifugal separation of a multispecies pure ion plasma. *Physics of Fluid*, 24(8):1447–1451, August 1981.

[20] T.G. Northrop and E. Teller. Stability of the adiabatic motion of charged particles in the earth's field. *Physical Review II*, 117(1):215–225, January 1960.

[21] Francis Robicheaux. private communications, 2009.

[22] E.P. Gilson and J. Fajans. Quadrupole-induced resonant-particle transport in a pure electron plasma. *Physical Review Letters*, 90(1):015001, January 2003.

[23] K. Gomberoff et al. Simulations of plasma confinement in an antihydrogen trap. *Physics of Plasmas*, 14(10):102111, October 2007.